Thiopurines inhibit coronavirus Spike protein processing and incorporation into progeny virions

Eric S. Pringle [1,*], Brett A. Duguay [1,*], Maxwell P. Bui-Marinos [2,3], Rory P. Mulloy [2,3], Shelby L. Landreth [4,5], Krishna Swaroop Desireddy [6], Stacia M. Dolliver [1], Shan Ying [1], Taylor Caddell [1], Patrick D. Slaine [1], Stephen L. Bearne [6,7], Darryl Falzarano [4,5], Jennifer A. Corcoran [2,3], Denys A. Khaperskyy [1,#], Craig McCormick [1,#]

[1]Department of Microbiology & Immunology, Dalhousie University, 5850 College Street, Halifax NS, Canada B3H 4R2

[2]Department of Microbiology, Immunology and Infectious Diseases, University of Calgary, 2500 University Drive NW, Calgary AB, Canada T2N 1N4

[3]Snyder Institute for Chronic Diseases and Charbonneau Institute of Cancer Research, University of Calgary, 2500 University Drive NW, Calgary AB, Canada T2N 1N4

[4]Department of Veterinary Microbiology, Western College of Veterinary Medicine, University of Saskatchewan, 52 Campus Drive, Saskatoon SK, Canada S7N 5E3

[5]Vaccine and Infectious Disease Organization (VIDO), 120 Veterinary Road, Saskatoon SK, Canada S7N 5E3

[6]Department of Biochemistry and Molecular Biology, Dalhousie University, Halifax, NS, Canada B3H 4R2

[7]Department of Chemistry, Dalhousie University, Halifax, NS, B3H 4R2, Canada

*Co-lead authors

[#]Co-corresponding authors: D.A.K., D.Khaperskyy@dal.ca, C.M., craig.mccormick@dal.ca

Running Title: Thiopurines inhibit coronavirus Spike glycoprotein processing

Keywords: virus, coronavirus, SARS-CoV-2, HCoV-229E, HCoV-OC43, thiopurine, 6-thioguanine, 6-thioguanosine, unfolded protein response, glycosylation, Spike, assembly, GTPase, host-targeted antiviral

ABSTRACT

There is an outstanding need for broadly acting antiviral drugs to combat emerging viral diseases. Here, we report that thiopurines inhibit the replication of the betacoronaviruses HCoV-OC43 and SARS-CoV-2, and to a lesser extent, the alphacoronavirus HCoV-229E. 6-Thioguanine (6-TG) disrupted early stages of infection, limiting synthesis of full-length and subgenomic HCoV RNAs. Furthermore, consistent with our previous report on the effects of thiopurines on influenza A virus glycoproteins, we observed that 6-TG inhibited accumulation of Spike glycoproteins from diverse HCoVs. Specifically, 6-TG treatment decreased the accumulation of Spike proteins and increased their electrophoretic mobility, consistent with Spike migration following the enzymatic removal of N-linked oligosaccharides with Peptide:N-glycosidase F (PNGaseF). SARS-CoV-2 virus-like particles (VLPs) harvested from 6-TG-treated cells were deficient in Spike. 6-TG treatment had a similar effect on lentiviruses pseudotyped with SARS-CoV-2 Spike; lentiviruses could be harvested from cell supernatants but were deficient in Spike and unable to infect human cells bearing ACE2 receptors. Together, these findings from complementary ectopic expression and infection models strongly indicate that defective Spike trafficking and processing is an outcome of 6-TG treatment. At low micromolar doses, the primary known mode of action of 6-TG is selective inhibition of the small GTPase Rac1. However, we observed that selective chemical inhibitors of the small GTPases Rac1, CDC42 and Rho had no effect on Spike processing and accumulation. The GTPase agonist ML099 countered the effects of 6-TG, suggesting that an unknown GTPase could be the relevant 6-TG-target protein involved in regulating Spike processing and accumulation. Overall, these findings provide important clues about the mechanism of action of a candidate antiviral that can broadly target HCoVs and suggest that small GTPases are promising targets for host-targeted antivirals.

55 **AUTHOR SUMMARY**
56 The COVID-19 pandemic has ignited efforts to repurpose existing drugs as safe and effective
57 antivirals. Rather than directly inhibiting viral enzymes, host-targeted antivirals inhibit host cell
58 processes to indirectly impede viral replication and/or stimulate antiviral responses. Here, we
59 describe a new antiviral mechanism of action for the FDA-approved thiopurine 6-thioguanine. We
60 demonstrate that this thiopurine is a pro-drug that must be metabolized by host enzymes to gain
61 antiviral activity. We show that it can inhibit the replication of several human coronaviruses,
62 including SARS-CoV-2, at least in part by interfering with the processing and accumulation of
63 Spike glycoproteins, thereby impeding assembly of infectious progeny viruses. We provide
64 evidence implicating host cell GTPase enzymes in the antiviral mechanism of action.

65

66 **INTRODUCTION**

67 Coronaviruses (CoVs) are enveloped viruses with positive-sense, single-stranded RNA
68 ((+)ssRNA) genomes. Seven human CoVs (HCoVs) are divided into two genera, the
69 alphacoronaviruses (HCoV-NL63 and HCoV-229E) and betacoronaviruses (HCoV-OC43, HCoV-
70 HKU1, MERS-CoV, SARS-CoV and SARS-CoV-2). Following entry into host cells, the
71 (+)ssRNA CoV genome is immediately translated into polyproteins that are cleaved by viral
72 cysteine proteases into 16 non-structural proteins (NSPs). These NSPs include the transmembrane
73 nsp3-nsp4-nsp6 complex that generates a complex endoplasmic reticulum (ER)-derived
74 reticulovesicular network that includes replication organelles known as double-membrane vesicles
75 (DMVs) (1–8). In DMVs, the nsp3-nsp4-nsp6 complex provides a physical anchor for the viral
76 replicase-transcriptase complex (RTC) that replicates the large viral genome and synthesizes
77 subgenomic mRNAs (9, 10). These viral RNAs traverse a crown-shaped pore to exit the DMV (8).
78 In the cytoplasm, viral mRNAs are translated into structural proteins; Nucleocapsid (N) is
79 synthesized via free ribosomes in the cytoplasm, whereas mRNAs encoding envelope proteins are
80 translated and processed in the ER and accumulate in the ER-Golgi-intermediate compartment
81 (ERGIC). HCoV assembly takes place when full-length viral genomic RNA coated with N buds
82 into the ERGIC to acquire the viral envelope and associated envelope proteins (11–13). These
83 progeny viruses traverse the Golgi apparatus and *trans*-Golgi network (TGN), where envelope

84 proteins receive additional post-translational modifications, and exit the cell via lysosomal
85 exocytosis (14).

86 CoV envelope proteins are subject to extensive processing in the secretory pathway. The
87 viral envelope proteins Spike, Envelope (E) and Matrix (M) that are found in all HCoVs, as well
88 as Hemagglutinin-Esterase (H-E) found in only HCoV-OC43 and HCoV-HKU1, are synthesized
89 in the ER as transmembrane proteins (15). CoV Spike proteins are large type I transmembrane
90 proteins that are heavily N-glycosylated, which promotes proper folding, trimerization and
91 trafficking (16). Subsequent proteolytic processing is required to activate these glycosylated Spike
92 trimers, generating the S1 attachment subunit and liberating the mature amino-terminal fusion
93 peptide of the S2 subunit, both of which are essential components of infectious CoV virions that
94 can enter target cells (17, 18). Proteolytic activation of Spike can occur in the secretory pathway
95 of infected cells or unprocessed Spike can be incorporated into virions and Spike processing can
96 occur during attachment and entry into naïve cells in a process that involves multiple host serine
97 and cysteine proteases. M is the most abundant CoV envelope protein and it serves as a scaffold
98 for viral assembly. It is a multi-spanning membrane protein, with a small lumenal amino-terminus
99 that is N-glycosylated, three transmembrane domains, and a large cytoplasmic carboxy-terminal
100 domain known as the endodomain that governs interactions with the other structural proteins
101 (Spike, E and N), as well as M-M interactions (19). E is a small type I transmembrane protein that
102 forms pentameric complexes and functions as a viroporin, increasing the lumenal pH in the Golgi
103 and protecting Spike from proteolysis (reviewed in (20)). The viroporin activity may support de-
104 acidification of lysosomes and subsequent lysosomal exocytosis. M and E proteins both govern
105 the intracellular trafficking and processing of Spike (19).

106 The striking remodeling of the ER to create replication organelles, as well as the reliance
107 on the ER for synthesis and processing of viral glycoproteins, has prompted investigations into the
108 effects of HCoV infection on ER stress and the unfolded protein response (UPR). Several CoVs
109 have been shown to activate the UPR, including infectious bronchitis virus (IBV) (21, 22), mouse
110 hepatitis virus (MHV) (23), transmissible gastroenteritis virus (TGEV) (24), HCoV-OC43 (25)
111 and SARS-CoV (26–28). However, proximal UPR sensor activation does not always elicit
112 downstream UPR transcription responses during CoV replication (29), which suggests complex
113 regulation of the UPR by certain CoVs. Spike proteins from MHV (23), HCoV-HKU1 (27) and
114 SARS-CoV (27, 30) are sufficient for UPR activation in cell culture. Additional transmembrane

115 CoV proteins also induce the UPR, including SARS-CoV non-structural protein 6 (nsp6) (31),
116 ORF3a (32) and ORF8ab (33) proteins. Despite these discoveries, our understanding of the
117 regulation of the UPR in CoV infection remains incomplete, and little is known about UPR
118 regulation in SARS-CoV-2 infection.

119 The emergence of SARS-CoV and MERS-CoV from animal reservoirs, followed by the
120 current SARS-CoV-2 pandemic, has spurred efforts to discover and develop effective antivirals.
121 These efforts have benefitted from drug repurposing strategies to identify antivirals amongst drugs
122 that have already been approved for use in humans. We showed previously that thiopurines 6-
123 thioguanine (6-TG) and 6-thioguanosine (6-TGo) selectively inhibit influenza A virus (IAV)
124 replication by activating the UPR and interfering with the processing and accumulation of viral
125 glycoproteins (34). Thiopurines have been in clinical use for over 50 years to treat inflammatory
126 diseases and cancer and as immunomodulators. They include azathioprine, 6-mercaptopurine (6-
127 MP) and 6-TG. 6-TG is orally bioavailable and on the World Health Organization's List of
128 Essential Medicines. It is used to treat hematological malignancies, including acute lymphoblastic
129 leukemia (AML), acute lymphocytic leukemia (ALL) and chronic myeloid leukemia (CML), with
130 the primary mechanism of action involving conversion into thioguanine deoxynucleotides and
131 incorporation into cellular DNA, which preferentially kills rapidly dividing cancer cells (35, 36).
132 By contrast, the anti-inflammatory effect of sub-cytotoxic doses of 6-TG for treating inflammatory
133 bowel disease (IBD) is thought to be primarily due to inhibition of the small GTPase Rac1 (37,
134 38). This process requires 6-TG to be metabolized by the purine scavenging enzyme hypoxanthine
135 phosphoribosyltransferase 1 (HPRT1) to yield 6-thioguanosine 5'-monophosphate (6-TGMP),
136 which is then converted to 6-thioguanosine 5'-triphosphate (6-TGTP). 6-TGTP is the active
137 metabolite that covalently modifies a reactive cysteine in the p-loop of Rac1. Subsequent
138 hydrolysis of the GTPase-bound 6-TGTP adduct yields a trapped, inactive Rac1-6-TGDP product
139 (37). These host-targeted properties of 6-TG, combined with our knowledge of how 6-TG inhibits
140 IAV glycoprotein processing, motivated us to investigate whether 6-TG and related thiopurines
141 might similarly interfere with CoV glycoproteins. Moreover, we reasoned that this kind of host-
142 targeted antiviral activity might act synergistically with the previously reported direct-acting
143 antiviral activity of 6-TG as an inhibitor of MERS-CoV, SARS-CoV and SARS-CoV-2 papain-
144 like cysteine proteases PL^{pro} (nsp3) *in vitro* (39–42). Using ectopic expression and cell culture
145 infection models, we discovered that 6-TG and 6-TGo inhibits replication of several CoVs

146 including SARS-CoV-2, which correlates with disruption of Spike processing, as well as Spike
147 accumulation and incorporation into progeny virions. Accumulation of viral subgenomic RNAs
148 and full-length genomes is also inhibited by these thiopurines. Finally, we were able to link the
149 antiviral mechanism of action to the primary known mode of action of 6-TG and related molecules
150 as selective inhibitors of small GTPases (37, 43, 44), which could be overcome using a pan-
151 GTPase agonist. Our findings extend the understanding of the mechanism of action of these
152 candidate host-targeted antivirals and provide a means to study the impact of glycoprotein
153 maturation on coronavirus biology.

154

155 **RESULTS**

156 **6-Thioguanine and 6-thioguanosine inhibit HCoV replication**. We tested the effects of three
157 thiopurines (**Fig. 1A**) on SARS-CoV-2 replication in Calu-3 lung adenocarcinoma cells. Treatment
158 with 6-TG, the ribonucleoside 6-TGo, or the related thiopurine 6-MP, caused a striking 4-log
159 decrease in the release of infectious virions after 48 h of infection, with little effect on cell viability
160 [Selectivity Index (SI) 6-TG > 72,7, 6-Tgo > 81.6, 6-MP >153.8] (**Figs. 1B, 1C**). The sub-
161 micromolar EC_{50} values that we observed for all three thiopurines in the Calu-3 infection model
162 were consistent with previously reported values from other groups (42, 45). 6-TG was well
163 tolerated in three other cell lines we used for HCoV infection models (HCT-8, Huh7.5, and primary
164 hTERT-immortalized fibroblasts) (**Fig. 1D**). We tested the ability of 6-TG to inhibit the
165 betacoronavirus HCoV-OC43 and the alphacoronavirus HCoV-229E and found that low
166 micromolar doses of the ribonucleoside 6-TGo had similar inhibitory effects against HCoV-229E
167 and HCoV-OC43 in their respective infection models, whereas 6-MP had no effect **(Figs. 1E, 1F)**.
168 Because UPR stimulators thapsigargin (Tg) and tunicamycin (Tm) inhibit coronavirus replication
169 (46–49) and our previous work demonstrated that 6-TG can inhibit glycosylation of influenza A
170 virus (IAV) glycoproteins and stimulate ER stress (34), we included Tm as a positive control in
171 these studies. In hTERT-BJ cells, 6-TG inhibited HCoV-OC43 replication at low micromolar
172 doses, consistent with our observations in the HCT-8 cell infection model; however, HCoV-229E
173 replication in hTERT-BJ cells was minimally affected across a range of sub-cytotoxic
174 concentrations (**Figs. 1G, 1H**). Together, these findings suggest that 6-TG effectively inhibits
175 replication of several coronaviruses.

176

177 **6-Thioguanine impedes viral genome replication and subgenomic RNA synthesis.** Next, we
178 investigated which stages of virus replication were affected by 6-TG treatment. We performed
179 multi-round HCoV-OC43 infections of 293T cells at an MOI of 0.1. Infected cells were treated
180 with 10 μM 6-TG or DMSO immediately after infection, and cell lysates and supernatants were
181 harvested at regular intervals for the next 48 hours. 6-TG treatment caused a ~40-fold reduction in
182 viral titer during the first day of infection. Virion release from control cells plateaued at 24 hours
183 post-infection, whereas peak release of infectious virions from 6-TG-treated cells occurred much
184 later at 48 hours post-infection **(Fig. 2A)**. Similarly, measuring viral particle release by RT-qPCR
185 amplification of extracellular viral genomes revealed a ~20-fold reduction in virus titer **(Fig. 2B)**
186 throughout the first day of infection.

187 Next, we investigated the ability of 6-TG to disrupt viral RNA synthesis in infected cells.
188 Putative full-length RNA, as detected by primers targeting *ORF1a*, was reduced by ~10-fold
189 throughout most stages of infection. Similar decreases were detected using primers targeting the
190 coding region of *Spike* and *N* genes after 6 h post-infection, with much larger 40-fold differences
191 at 6 h post-infection **(Fig. 2C)**. Accumulation of viral proteins N and Spike was also inhibited (Fig.
192 2D). These disruptions in viral RNA accumulation correlated with changes in the localization of
193 N, the viral nucleoprotein. Immunostaining HCoV-OC43 infected cells with an anti-N antibody
194 revealed a punctate staining pattern at 6 hours post-infection **(Fig. 2E)**. By 24 h post-infection, N
195 immunostaining was less punctate and more peripheral. The N immunostaining was markedly
196 altered in 6-TG-treated infected cells, with brighter punctate staining patterns at 6 hours post-
197 infection and large puncta still visible at 24 h post-infection. The formation of replication
198 compartments was also delayed in 6-TG treated cells, as determined by immunostaining for
199 dsRNA **(Fig. 2F)**; Specifically, we observed dsRNA signal at 6 hpi, which correlated with
200 decreased viral RNA detected by RT-qPCR **(Fig. 2C)**. Together, these findings indicate that 6-TG
201 reduces the synthesis of viral RNAs required to support efficient HCoV replication.

202 In our recent study, the antiviral mechanism of action of 6-TG and 6-TGo against IAVs
203 involved activation of the UPR and interference with the processing and accumulation of viral
204 glycoproteins. In these experiments, IAV infection of vehicle-treated A549 cells revealed very
205 little detectable UPR late in infection at 24 h post-infection, whereas 6-TG stimulated all three

206 arms of the UPR, with transactivation of XBP1s target gene *Erdj4*, ATF6-N target genes *BiP* and
207 *HERPUD1* and ATF4 target gene *CHOP* (34). Thus, thiopurines markedly altered the ER
208 proteostasis landscape to the detriment of IAV replication. Notably, many HCoVs have been
209 shown to activate the UPR, including infectious bronchitis virus (IBV) (21, 22), mouse hepatitis
210 virus (MHV) (23), transmissible gastroenteritis virus (TGEV) (24), human coronavirus (HCoV)-
211 OC43 (25) and SARS-CoV (26–28). Here we show that HCoV-OC43 infection caused induction
212 of *Xbp1* transcript, potent accumulation of spliced Xbp1, and transactivation of XBP1s target genes
213 *Erdj4* and *Edem1*, providing strong evidence for activation of the IRE1 arms of the UPR **(Figs.**
214 **S1A, S1B)**. Regulation of the PERK/ATF4 arm of the UPR may be more complex, as HCoV-
215 OC43 infection caused accumulation of *ATF3* mRNA but no change in *CHOP*, even though they
216 are both encoded by ATF4 target genes. Similarly, we observed increased expression of ATF6-N
217 target genes *HERPUD1* and *Xbp1* but no increases in BiP mRNA or protein **(Figs. S1A, S1B)**.
218 Thus, HCoV-OC43 interactions with the UPR appear to be complex and marked by strong
219 stimulation of IRE1, which is consistent with observations from others (25). In marked contrast to
220 our IAV studies, 6-TG treatment generally delayed or suppressed the downstream UPR
221 transcriptional response **(Fig. S1A)**, which could be attributed to 6-TG-mediated delays in viral
222 replication and the accumulation of viral RNAs and proteins **(Fig. 2)**. Finally, it should be noted
223 that UPR transcripts accumulated to high levels in vehicle-treated cells despite the fact that HCoV-
224 OC43, like all HcoVs, has mechanisms to potently shut off host antiviral gene expression (25).
225 Using ribopuromycinylation assays, we demonstrated that HCoV-OC43 greatly reduced
226 translation of host mRNAs at the expense of viral mRNAs encoding a few abundant viral proteins
227 **(Fig. S1C, lane 4)**. 6-TG treatment had no effect on global rates of translation initiation in HCoV-
228 OC43 infected cells, with the only changes evident being the apparent loss of some abundant viral
229 proteins **(Fig. S1C, lane 6)**. Together, these observations suggested that 6-TG inhibition of HCoV-
230 OC43 infection limits the strong activation of IRE1 and accumulation of XBP1s target genes, and
231 that even though 6-TG interferes with synthesis of viral full-length genomic RNAs and
232 subgenomic RNAs, host shutoff is unperturbed.

233

234 **6-Thioguanine inhibits Spike processing and accumulation.** We previously reported that 6-TG
235 and 6-TGo inhibited the processing and accumulation of IAV glycoproteins hemagglutinin (HA)
236 and neuraminidase (NA) (34). Here, we observed a similar defect in SARS-CoV-2 infected cells;

237 lysates harvested from SARS-CoV-2-infected Calu-3 cells at 48 h post-infection showed a sharp
238 decrease in all four structural proteins following 6-TG treatment **(Fig. 3A)**, consistent with a sub-
239 micromolar EC50 discussed above **(Fig. 1B)**. Treatment of SARS-CoV-2-infected Huh-7.5 cells
240 with 10 μM 6-TG also reduced the accumulation of viral structural proteins, which was especially
241 evident for Spike **(Fig. 3B)**. These findings led us to further investigate the effects of 6-TG on
242 SARS-CoV-2 structural proteins. Transfection of 293T cells with plasmids encoding each SARS-
243 CoV-2 structural protein revealed that 6-TG had no effect on E or N accumulation, whereas Spike
244 processing was noticeably inhibited (**Fig. 3C**). We also observed that 6-TG treatment caused a loss
245 of a slow-migrating species of M **(Fig. 3C)**, which likely represented the glycosylated form of the
246 protein that has been previously reported for other HCoVs (50). Thus, it appears that amongst the
247 SARS-CoV-2 structural proteins, only the glycosylated Spike and M proteins are altered by 6-TG
248 treatment when expressed independently in 293T cells.

249 To further explore the effects of 6-TG on Spike, we ectopically expressed Spike, then
250 treated the cells with a range of sub-cytotoxic 6-TG concentrations before harvesting lysates and
251 processing for immunoblotting **(Figs. 3D, 3E)**. Spike appeared as two bands when immunoblots
252 are probed with an anti-S1 receptor binding domain (RBD) antibody, a high-molecular weight
253 (MW) precursor S0 band (~203 kDa) and a lower molecular weight band representing the protease-
254 cleaved S1 attachment protein (~96 kDa). Increasing concentrations of 6-TG once again led to the
255 accumulation of a prominent single band at an unexpected MW (~137 kDa) **(Fig. 3D)**. Because 6-
256 TG treatment caused Spike to migrate faster during SDS-PAGE than expected, we hypothesized
257 that the lower MW species observed only in 6-TG treated samples could arise from a glycosylation
258 defect. We treated lysates from Spike-expressing 293T cells with Peptide-*N*-Glycosidase F
259 (PNGase F), an amidase that cleaves the bond between N-acetylglucosamine (GlcNAc) and
260 asparagine, effectively removing all N-linked glycans from the polypeptide chain (unless the core
261 GlcNAc is modified by α-1,3-fucose) (51). PNGase F treatment caused Spike from the DMSO-
262 treated cells to migrate similarly to Spike from 6-TG-treated cells **(Fig. 3F)**. We confirmed the
263 identity of the high MW Spike band as the uncleaved S0 precursor protein by generating and
264 testing a mutant Spike protein in which the basic residues in the furin cleavage site joining S1 and
265 S2 were substituted with alanines, yielding a protease cleavage-resistant Spike protein. Cells
266 transfected with this S0 construct and treated with 6-TG prior to lysis revealed that the S0 construct
267 was also sensitive to PNGaseF treatment; the 6-TG/PNGaseF-treated S0 migrated similarly to 6-

268 TG/PNGaseF-treated WT Spike by SDS-PAGE. Several studies have mapped O-linked glycans
269 on SARS-CoV-2 Spike (52–54) and these modifications appear to follow the "O-follow-N rule"
270 whereby N-glycosylation is followed by O-glycosylation on nearby residues (52). Thus, the
271 apparent differences in molecular weight between vehicle/PNGaseF-treated Spike and 6-
272 TG/PNGaseF-treated Spike could stem from residual O-linked glycans on Spike that are absent in
273 the 6-TG-treated proteins. These findings were corroborated using carboxy-terminal FLAG-tagged
274 Spike proteins from SARS-CoV-2 and MERS-CoV that also displayed a fast-migrating, under-
275 glycosylated S0 species and loss of the S2 subunit following 6-TG treatment **(Fig. 3G)**. Taken
276 together, these results suggest that 6-TG inhibits normal glycosylation and processing of Spike.

277 A failure of Spike to migrate efficiently from the ER to the Golgi could inhibit glycan
278 maturation and cleavage by furin. In our previous work, we observed that 6-TG treatment did not
279 reduce levels of Class I HLA proteins at the cell surface (34), which we interpreted as evidence
280 that 6-TG did not globally affect processing and secretion of host cell glycoproteins. Here, we
281 tested the role of 6-TG on the secretory pathway by using a *Gaussia* luciferase assay in which the
282 enzyme depends on a native secretion signal to be secreted (55). As a control we used the Arf1-
283 inhibitor brefeldin A (BFA) which potently inhibits protein trafficking from the ER to the Golgi
284 (56, 57). BFA is toxic to cells at micromolar doses, but we could still detect secretory pathway
285 inhibition at 250 nM for 20 h without overt cytotoxicity **(Figs. S2A, S2B)**. A short-term, 6 h
286 treatment with 6-TG (10 μM) had little effect on *Gaussia* luciferase secretion, whereas treatment
287 with BFA (10 μM) greatly decreased secretion. We tested a longer 20 h treatment of 6-TG where
288 we co-transfected Firefly luciferase (Luc2) with *Gaussia* luciferase to help control for the
289 inhibitory effects of 6-TG on 293T cell proliferation. This extended 6-TG treatment caused a slight
290 loss of detectable *Gaussia* luciferase activity in the cell supernatant, but once again low-dose
291 treatment of BFA greatly inhibited secretion and increased intracellular retention of *Gaussia*
292 luciferase (**Fig. S2C**). These experiments strongly corroborated our prior observations that 6-TG
293 treatment does not globally disrupt the secretory pathway. Because of our previous observations
294 of 6-TG-mediated defects in Spike glycosylation, processing and trafficking, we decided to test
295 whether low-dose, long-term treatment with BFA would be sufficient to recapitulate the effects of
296 6-TG treatment on Spike. However, unlike 6-TG, the secretion inhibitor BFA did not cause any
297 changes in Spike accumulation or processing, as indicated by identical electrophoretic mobility of
298 Spike on immunoblots compared to vehicle control **(Fig. S2D).**

299 To directly monitor Spike protein secretion, we used flow cytometry and surface staining
300 of unpermeablized 293T cells transfected with Spike. We co-transfected cells with an EGFP
301 plasmid and gated on EGFP+ cells to measure changes in Spike accumulation. 6-TG reduced
302 surface expression of Spike by ~50% resulting in fewer Spike-positive cells and reduced mean
303 fluorescence intensity. In these experiments, we also tested a Spike protein in which the 19 C-
304 terminal residues were removed (Spike-Δ19); this widely-used strategy removes an ER-retrieval
305 signal and enhances incorporation of Spike into lentivirus particles (58–60). We found a similar
306 ~50% reduction in trafficking and surface expression of Spike-Δ19 **(Fig. S2E)**. Together, these
307 experiments indicate that 6TG inhibits normal trafficking of Spike to the cell surface but does not
308 broadly inhibit secretion.

309

310 **6-Thioguanine causes a coronavirus assembly defect.** It has been shown that co-transfection of
311 plasmids expressing each of the four SARS-CoV-2 structural proteins allows for secretion of virus-
312 like particles (VLPs) (19), which is concordant with earlier studies with other CoV structural
313 proteins (61). However, we observed that when Spike, E, M and N expression vectors were co-
314 transfected into cells, 6-TG treatment not only altered the accumulation and processing of Spike,
315 but also dramatically reduced accumulation of E and M proteins (**Fig. 4A**). Cell supernatants were
316 collected, filtered and pelleted in a sucrose cushion to isolate VLPs, which were then characterized
317 by immunoblotting. We observed a dramatic reduction in VLP production from 6-TG-treated 293T
318 cells, and these residual VLPs completely lacked Spike (**Fig. 4B**). These findings indicate that 6-
319 TG not only prevents Spike processing and accumulation, but also its incorporation into VLPs.
320 We then co-transfected cells again with only three of the four Spike, E, M, and N encoding
321 plasmids to better understand mechanisms of defective assembly. Our main conclusions are: 1) 6-
322 TG treatment of cells expressing all structural proteins causes a strong Spike-dependent decrease
323 in E expression, 2) in the absence of M the 6-TG-mediated Spike glycosylation defect is more
324 pronounced, and 3) N is required for accumulation of E **(Fig 4C)**. To determine if Spike from 6-
325 TG treated cells was still functional, we employed a lentivirus pseudotyping method using Spike-
326 Δ19, which is widely used to measure neutralizing antibody titers to SARS-CoV-2 (58, 62, 63).
327 We performed immunoblots on pseudotyped viruses (PVs) recovered from three independent
328 preparations that we purified by ultracentrifugation through a 20% sucrose cushion. Unlike our
329 previous immunoblots of ectopically expressed Spike from transfected cells, we observed that

330 most of the Spike proteins incorporated into the PVs were fully cleaved into the prominent S1
331 band **(Fig. 4D)**. However, 6-TG treatment led to a dramatic loss of Spike S0 and S1 species from
332 the purified PVs, compared to the smaller decrease observed for HIV p24 levels in PV cores. We
333 quantified PV yield from these cells by amplifying lentiviral genomes via RT-qPCR from filtered,
334 unconcentrated cell supernatants. 6-TG treatment did not significantly reduce the quantity of
335 capsid-protected genomes released from cells compared to vehicle control **(Fig. 4E)**. To determine
336 the effects of 6-TG on PV infectivity, we used purified PVs to infect HEK293A cells that stably
337 express the ACE2 receptor and measured luciferase production in the recipient cells as a measure
338 of successful lentiviral infection. Consistent with deficient Spike incorporation into PVs, we
339 observed that 6-TG treatment reduced PV infectivity by over 50-fold compared to PVs derived
340 from vehicle-treated cells **(Fig. 4F)**. By contrast, PVs derived from vehicle control- and 6-TG-
341 treated cells were equally competent to infect ACE2-deficient HEK293A cells at low levels. This
342 suggests that 6-TG treatment not only inhibits Spike glycosylation and processing, but it also
343 inhibits Spike trafficking and incorporation into lentiviral particles. We next investigated whether
344 these 6-TG-mediated assembly defects altered the morphology of HCoV particles. We
345 concentrated supernatant from HCoV-OC43 infected 293A cells by ultracentrifugation and imaged
346 virions by transmission electron microscopy using negative staining. We observed fewer viral
347 particles in the 6-TG treated samples, and while these particles were of similar size, we noted fewer
348 particles with clearly discernible Spikes **(Fig. 4G)**. Taken together, the strong effects of 6-TG on
349 Spike in transiently transfected cells, heterologous lentivirus production and infection, and
350 authentic HCoV infections, provide evidence for an additional antiviral mode of action for 6-TG
351 beyond PLpro/nsp3 inhibition or defects in viral RNA synthesis.

352

353 **6-Thioguanine must be processed by HPRT1 to inhibit Spike processing and coronavirus**
354 **replication.** We observed comparable antiviral activities of 6-TG and its ribose-conjugated
355 analogue 6-TGo throughout these studies. Metabolism of 6-TG is initiated by the purine
356 scavenging enzyme hypoxanthine phosphoribosyltransferase 1 (HPRT1) to yield 6-thioguanosine
357 5'-monophosphate (6-TGMP) **(Fig. 5A)**. 6-TGMP can then be converted to 6-thioguanosine 5'-
358 triphosphate (6-TGTP), the active form of the molecule that has been shown to form a covalent
359 bond with a reactive cysteine in the p-loop of Rac1; subsequent hydrolysis of Rac1-6-TGTP to a
360 diphosphate form renders the GTPase inactive (37). Considering this information, we next sought

361 to determine whether conversion of 6-TG to a ribonucleoside was required for its antiviral activity.
362 First, we synthesized N9-methyl 6-thioguanine (6-TG-Me), which prevents conjugation to a ribose
363 sugar due to the methyl group at N9 of the purine ring and is predicted to be resistant to conversion
364 into 6-TGMP **(Fig. 5A)**. 6-TG-Me displayed low cytotoxicity and no antiviral activity against
365 HCoV-OC43 across a broad range of concentrations **(Fig. 5B)**. Likewise, 6-TG-Me had no effect
366 on SARS-CoV-2 Spike processing across a range of concentrations between 5 μM and 20 μM
367 **(Fig. 5C)**. To corroborate this finding, we used RNA interference to silence expression of *HPRT1*
368 in 293T cells prior to infection with HCoV-OC43 and treatment with 6-TG or vehicle control. RT-
369 qPCR confirmed effective silencing of *HPRT1* **(Fig. 5D)**, which had no effect on HCoV-OC43
370 infection in vehicle control-treated cells **(Fig. 5E)**. By contrast, *HPRT1* silencing significantly
371 restored viral replication in the presence of 6-TG, although replication did not return to the levels
372 in control cells. Together, these findings indicate that 6-TG is a pro-drug that must be metabolized
373 by HPRT1 to convert it to an active form.

374

375 **6-Thioguanine inhibits Spike maturation by inhibiting an unidentified cellular GTPase.** 6-
376 TG inhibits several different GTPases including Rac1, RhoA, and Cdc42 (37, 43, 44). This mode
377 of action was previously shown to inhibit rotavirus replication at sub-micromolar concentrations
378 (64). Here, we sought to determine if any of the known targets of 6-TG were responsible for defects
379 in Spike maturation. We tested known inhibitors of Rac1 (Rac1 Inhibitor V), RhoA (Rhosin), and
380 Cdc42 (CASIN) for cytotoxic effects in 293T cells after 24 h incubation using an alamarBlue assay
381 to identify optimal sub-cytotoxic doses for further testing (**Figs. 6A, 6B)**. We also tested a GTPase
382 agonist ML099 that can potently activate Rac1, RhoA, and Cdc42, among other GTPases (65).
383 None of the three GTPase inhibitors had any effect on Spike processing or accumulation **(Fig. 6C)**.
384 Because many additional GTPases have redox-sensitive cysteine residues that could interact with
385 6-TG, we reasoned that 6-TG could affect viral glycoproteins through an as-yet-unidentified
386 GTPase. In support of this notion, we observed that the broadly acting small GTPase agonist
387 ML099 maintained normal Spike processing in the presence of 6-TG **(Fig. 6D)**. Pre-treating the
388 cells with ML099 before addition of 6-TG further enhanced this effect **(Fig. 6E)**. We attempted to
389 rescue HCoV-OC43 titer in both HCT-8 and 293A infection models but instead found that ML099
390 was itself acting as an antiviral agent **(Fig. 6F)**. While this was worth testing, this result was

391 unsurprising as viral infection likely requires specific or unperturbed GTPase function, including
392 frequent cycling between GTP- and GDP-bound forms. Overall, these data suggest that 6-TG
393 inhibits Spike maturation by inhibiting an unidentified cellular GTPase.

394

395 **DISCUSSION**

396 The reliance of viruses on the host cell biosynthetic and secretory apparatus, combined with the
397 existence of varied and potent host antiviral mechanisms, makes host targeted antivirals (HTAs)
398 useful additions to our armamentarium of direct-acting antivirals (DAAs). By targeting these host
399 cell processes, HTAs may not be so easily subverted by the rapid viral evolution that frequently
400 undermines DAAs. We recently reported that the thiopurines 6-TG and 6-TGo inhibit influenza A
401 virus (IAV) by selectively disrupting the normal processing and accumulation of HA and NA
402 glycoproteins (34). We hypothesized that other enveloped viruses that rapidly produce a burst of
403 viral glycoproteins would also be susceptible to these thiopurines. Here, we report that the
404 thioguanine 6-TG disrupts the normal processing and accumulation of CoV Spike glycoproteins
405 and inhibits the release of infectious progeny. This drug-induced Spike processing defect disrupts
406 the incorporation of SARS-CoV-2 Spike into VLPs or pseudotyped lentiviruses, which
407 subsequently prevents infection of susceptible, ACE2-expressing cells. Thiopurines inhibit the
408 small GTPase Rac1 by forming a covalent bond with a redox-sensitive cysteine, preventing further
409 guanine nucleotide exchange. However, we show that selective chemical inhibitors of Rac1 or
410 related small GTPases CDC42 and Rho had no effect on Spike processing and accumulation,
411 whereas a broad GTPase agonist was able to counter the effects of 6-TG. This indicates that there
412 are additional, unknown GTPase targets of 6-TG and that these are required for normal Spike
413 processing and accumulation. Together, these findings suggest that functional small GTPases are
414 essential for virus replication and that further development of GTPase inhibitors as host-directed
415 antivirals is warranted.

416 We were intrigued by how 6-TG and 6-TGo strongly inhibited processing and
417 accumulation of IAV and CoV glycoproteins. However, we also observed that these thiopurines
418 had little effect on global host protein synthesis and secretion. Together, these observations suggest
419 that viral glycoproteins may have properties that make them especially sensitive to these drugs.
420 Certainly, viral glycoproteins must adhere to temporal or physical constraints that most host

421 glycoproteins do not. All glycoproteins are synthesized, folded and post-translationally modified
422 in the ER. However, viral glycoproteins can impose an acute burden on the ER when they are
423 rapidly synthesized in large numbers in a relatively brief time frame. This burden may differ in
424 severity depending on the extent of shutoff of host gene expression, as viruses with efficient host
425 shutoff mechanisms would deplete host glycoproteins and facilitate viral utilization of the cellular
426 biosynthetic and secretory apparatus. Viral envelope proteins are often more heavily glycosylated
427 than their host counterparts, which can shield them from antibody recognition. Because N-
428 glycosylation is a dynamic process involving glycan trimming and maturation, viral infection may
429 impose specific burdens on these components of the ER quality control machinery. This may result
430 in delayed trafficking of glycoproteins through the secretory pathway, leading to their degradation.
431 Finally, it should be noted that viral glycoproteins are often assembled into large homo- and hetero-
432 oligomeric complexes that must traffic to sites of assembly. Together, these aspects of viral
433 glycoprotein biology place additional burdens on the ER and the associated machinery that governs
434 glycoprotein folding, modification and trafficking.

435 Because cellular GTPases play important roles in viral glycoprotein biogenesis and
436 trafficking, they may be good targets for host-directed antivirals. Viral assembly occurs at distinct
437 sites like the plasma membrane (influenza A viruses) or the ERGIC (coronaviruses). Small
438 molecules that disrupt efficient viral glycoprotein processing, oligomerization and trafficking
439 could have the effect of 'misplacing' these important viral components and inhibiting essential
440 steps in viral assembly and egress. We speculate that 6-TG and 6-TGo inhibit GTPases involved
441 in key steps of viral glycoprotein synthesis, processing and trafficking, diverting them from their
442 roles in viral assembly and consigning them to degradation via cellular catabolic processes. While
443 these drugs are well-tolerated in humans, we believe that more can be gained by identifying new
444 target GTPase(s) and further elucidating the antiviral mechanism of action to inform the
445 development of novel chemical entities with superior properties.

446

447 **MATERIALS AND METHODS**

448 **Cell lines.** Human embryonic kidney 293T and 293A cells, human hepatoma Huh-7.5 (66) and
449 African green monkey kidney Vero cells were all maintained in Dulbecco's modified Eagle's
450 medium (DMEM; ThermoFisher, 11965118) supplemented with heat-inactivated 10% fetal bovine
451 serum (FBS, ThermoFisher, A31607-01), 100 U/mL penicillin, 100 µg/mL streptomycin, and 2
452 mM L-glutamine (Pen/Strep/Gln; ThermoFisher, 15140122 and 25030081). HCT-8 cells were
453 cultured as above with additional 1X MEM Non-Essential Amino Acids (NEAA, ThermoFisher)
454 supplemented. Baby hamster kidney (BHK-21) were maintained as above yet supplemented with
455 5% FBS. African green monkey kidney Vero'76 and human lung adenocarcinoma Calu-3 cells
456 were maintained in DMEM (Sigma-Aldrich, D5796; St. Louis, MO, USA) supplemented with
457 10% fetal bovine serum (ThermoFisher, 16000-044) and 1X Penicillin-Streptomycin
458 (ThermoFisher, 15140148). hTert-immortalized human foreskin fibroblast (BJ) cells (a kind gift
459 from William Hahn, Dana-Farber Cancer Institute, Boston, USA) cells were maintained in a 4:1
460 blend of knockout DMEM (ThermoFisher, 10829-018) and Medium 199 (ThermoFisher, 11150-
461 059) with 15% FBS and Pen/Strep/Gln. All cells were maintained at 37°C in 5% CO_2 atmosphere.
462 To generate 293A-ACE2 cells, 293A cells were stably transduced with a lentivirus vector encoding
463 ACE2 (pLJM1-ACE2-BSD) or an empty vector control (pLJM1-B*) (67), then selected and
464 maintained in 10 µg/mL Blasticidin S HCl (ThermoFisher, A11139030).
465

466 **Chemical Inhibitors.** 6-thioguanine (6-TG, A4882), 2-amino-6-mercaptopurine riboside hydrate
467 (6-TGo, 858412), 6-mercaptopurine (6-MP, 38171), brefeldin A (BFA; B7651), CASIN
468 (SML1253), ML-099 (SML1258), Rac1 inhibitor V (5308200001), rhosin (555460), thapsigargin
469 (Tg, cat#) and tunicamycin (Tm, cat#) were all purchased from Sigma-Aldrich. N9-methyl 6-
470 thioguanine (6-TG-Me) was synthesized as described in Supporting Information. All drugs were
471 solubilized in dimethyl sulfoxide (DMSO) and stored at -80˚C. Stock concentrations were diluted
472 to the indicated concentrations in cell culture media.
473

474 **Human coronavirus infections and quantitation.** Stocks of severe acute respiratory syndrome
475 coronavirus 2 (SARS-CoV-2) were propagated in Vero'76 cells (for strain SARS-CoV-
476 2/Canada/ON/VIDO-01/2020, used in Fig. 1A) or Vero E6 cells (SARS-CoV-2/SB3-TYAGNC,
477 used in Figs. 3A, 3B). To generate virus stocks, cells were infected at a low MOI for 1 h in serum-

478 free DMEM at 37°C following replacement of the inoculum with DMEM supplemented with 2%
479 FBS and 1X Pen/Strep and continued incubation at 37°C. Once CPE reached 75% at 2-3 d post-
480 infection, the viral supernatant was harvested, centrifuged at 5000 x *g* for 5 min, and then the
481 cleared viral supernatant was aliquoted and stored at -80°C. Stocks were titered by plaque assay
482 on Vero E6 cells (68) or TCID50 on Vero'76 cells with DMEM/2%FBS/Pen/Strep/Gln and
483 calculated using the Spearman-Kärber method.

484 Stocks of human coronavirus OC43 (hCoV-OC43; ATCC, VR-1558) were propagated in
485 Vero cells. Cells were infected at a MOI of 0.05 for 1 h at 33°C in serum-free DMEM. After 1 h,
486 the infected cells were maintained in DMEM supplemented with 1% FBS and Pen/Strep/Gln for
487 five days at 33°C. Upon harvest, the culture supernatant was centrifuged at 1000 x *g* for 5 min at
488 4°C, aliquoted, and stored at -80°C. Stocks of human coronavirus 229E (hCoV-229E; ATCC, VR-
489 740) were prepared similarly to hCoV-OC43 yet using Huh-7.5 cells and DMEM supplemented
490 with 2.5% FBS and Pen/Strep/Gln. Viral titers were enumerated by median tissue culture
491 infectious dose ($TCID_{50}$) assays. Following the serial dilution of the samples, the appropriate cell
492 line was infected for 1 h at 37°C prior to the replacement of the inoculum for the indicated overlay
493 medium and incubated at 37°C: BHK-21 cells (hCoV-OC43, DMEM/1%FBS/Pen/Strep/Gln) or
494 Huh-7.5 cells (hCoV-229E, DMEM/2.5%FBS/Pen/Strep/Gln). Viral titers were calculated using
495 the Spearman-Kärber method.

496 To test the effect of the indicated compounds on hCoV replication, 293A, 293T, BJ, Calu-
497 3, HCT-8, or Huh-7.5 cells were infected with hCoV diluted in serum-free DMEM at the indicated
498 MOI for 1 h. After 1 h, the inoculum was removed, replaced with DMEM/Pen/Strep/Gln
499 containing 1% FBS and NEAA (HCT-8), 2% FBS (Calu-3), 2.5% FBS (Huh-7.5, 293A or 293T),
500 or 5% FBS (BJ) supplemented with DMSO or drug at the indicated concentration, and maintained
501 for an additional 23 h. Infected BJ cells were incubated at 33°C during virus replication; all other
502 cells were incubated at 37°C. For infections of 293A, BJ, HCT-8, or Huh-7.5, the infected cells
503 were scraped into the culture medium, subjected to three freeze/thaw cycles, then stored at -80°C.
504 For SARS-CoV-2-infected Calu-3 cells or HCoV-OC43 infected 293T cells virus was collected
505 from culture supernatants at 48 h post-infection and stored at -80°C. Titers of hCoV-OC43, hCoV-
506 229E, and SARS-CoV-2 were determined using $TCID_{50}$ assays as indicated above.
507

508 **Cytotoxicity assays.** Cells seeded into 96-well tissue culture plates were treated with drugs diluted
509 at indicated concentrations and incubated with the cells for 20 h. At 20 h post-treatment, 10%
510 alamarBlue Cell Viability Reagent (ThermoFisher Scientific, DAL1025) diluted in
511 DMEM/Pen/Strep/Gln containing 1% FBS and NEAA (HCT-8), 2.5% FBS (Huh-7.5 or 293T), or
512 5% FBS (BJ) was added and further incubated for 4 h. Plates were read on FLUOstar Omega 96
513 well plate reader at an excitation of 544 nm, and an emission of 580-590 nm. Drug treatments were
514 then normalized to DMSO. For viability experiments using Calu-3 cells, cells grown in 96-well
515 plates were treated with drugs diluted at indicated concentrations and incubated with the cells for
516 48 h. At 48 h post-treatment, a one-fifth volume of CellTiter 96 AQueous One Solution Cell
517 Proliferation Assay (G3580, Promega) was added to DMEM/Pen/Strep containing 2% FBS and
518 incubated for 2 h. Plates were read at an absorbance of 490 nm with an xMark™ Microplate
519 Absorbance Spectrophotometer (Bio-Rad). Values were imported into GraphPad PRISM (v.9) and
520 CC_{50} values were calculated by fitting a non-linear curve to the data. Selectivity index (SI) was
521 calculated by dividing the IC_{50} (calculated above) by the CC_{50}.
522
523 **Real-time quantitative PCR.** Total RNA from cells was extracted using the RNeasy Plus Mini
524 Kit (QIAGEN, 74134) following the manufacturer's protocol. Synthesis of cDNA was performed
525 using the Maxima H Minus First Strand cDNA Synthesis Kit (ThermoFisher Scientific, K1652)
526 using random primers. Quantitative PCRs were performed using 200 nM primers, 1:250 (final)
527 diluted cDNA, and 1X GoTaq qPCR Master Mix (Promega, A6002). Amplifications were
528 performed using a CFX Connect Real-Time PCR Detection System (Bio-Rad) and Bio-Rad CFX
529 Manager 3.1 software. To measure supernatant virions, supernatant was mixed 1:1 with virus lysis
530 buffer [20 mM Tris HCl pH7.4, 300 mM NaCl, 2.5% NP-40, and 40 U/mL RNAaseOUT
531 (ThermoFisher)] for 5 min, then diluted 1:5 with nuclease-free water before 2 µL was used as
532 template in a 10 µL GoTaq 1-Step RT-qPCR (Promega, A6020) reaction (69). Primer sequences
533 are listed in Table 1.
534
535 **Immunofluorescence microscopy.** 293T were seeded on #1.5 coverslips (Zeiss, 411025-0003-
536 000) coated with poly-L-lysine (Sigma, P2658). The following day the cells were infected with
537 HCoV-OC43, to harvest the cells were washed once with 1x Dulbecco's PBS (ThermoFisher) and
538 fixed with 4% paraformaldehyde (Electron Microscopy Services, 15710) in PBS for 15 min at

539 room temperature. Coverslips were blocked and permeablized in staining buffer [1% human serum
540 (Sigma,4552) heat-inactivated at 56°C for 1h, 0.1% Triton X-100 PBS] for 1 h at room
541 temperature, then stained with 1:500 dilution anti-OC43 N (MAB9012, Millipore Sigma)
542 overnight at 4°C. The following day the coverslips were washed three times with PBS, then stained
543 with goat anti-mouse Alexa 488 (ThermoFisher, R37120) in staining buffer for 1 h at room
544 temperature in the dark. Coverslips were then counterstain for 5 min with Hoescht 33342
545 (ThermoFisher, 62249), washed three times with PBS, then mounted on coverglass using ProLong
546 Gold anti-fade reagent (ThermoFisher, P36930). Z-stacks were imaged on a Zeiss LSM880 and
547 processed into maximum intensity projections using Zen Black (Zeiss).

548

549 **Western Blotting.** Cell monolayers were washed once with ice-cold PBS and lysed in 2x Laemmli
550 buffer (4% [wt/vol] sodium dodecyl sulfate (SDS), 20% [vol/vol] glycerol, 120 mM Tris-HCl [pH
551 6.8]). DNA was sheared by repeated pipetting with a 21-gauge needle before adding 100 mM
552 dithiothreitol (DTT) and boiling at 95˚C for 5 min. Samples were stored at -20˚C until analysis.
553 Total protein concentration was determined by DC protein assay (Bio-Rad) and equal quantities
554 were loaded in each SDS-PAGE gel. For ribopuromycylation assays, a modified version of the
555 protocol by Schmidt, *et al.* (63) was used where the indicated samples were treated with 10 µg/ml
556 puromycin (ThermoFisher, A1113803) for 10 min, followed by a PBS wash, and lysate preparation
557 for immunoblotting as indicated above. Lysates from the ribopuromycylation assays were loaded
558 into gels prepared using the TGX Stain-Free FastCast Acrylamide Kit (Bio-Rad, 1610183) (Fig.
559 S1A). Lysates for quantitative Spike western blotting were loaded onto TGX Stain-Free 4-20%
560 gradient gels (Bio-Rad, 4568094) (Fig. 3D). Peptide-*N*-Glycosidase F (PNGase F; NEB, P0704)
561 treatment of lysates was performed as described in the manufacturer's directions. All proteins after
562 SDS-PAGE were transferred to polyvinylidene difluoride (PVDF) membranes (Bio-Rad) with the
563 Trans-Blot Turbo transfer apparatus (Bio-Rad). Membranes were blocked with 5% bovine serum
564 albumin in tris-buffered saline/0.1% [vol/vol] tween-20 (TBS-T) before probing overnight at 4˚C
565 with antibodies raised to the following targets: mouse anti-puromycin (Millipore-Sigma,
566 MABE343), mouse anti-OC43 N (CoV antibody, OC43 strain, clone 541-8F, Millipore-Sigma,
567 MAB9012), rabbit anti-OC43 S (Cusabio, CSB-PA336163EA-1HIY), rabbit anti-BiP (Cell
568 signaling Technologies (CST), mouse anti-XBP1s (CST, #12782), mouse anti-CHOP (CST,
569 #2895), rabbit anti-α-Tubulin (CST, #2125), rabbit anti-SARS-CoV-2 S1 RBD (Elabscience, E-

570 AB-V1006), anti-SARS-CoV-2 E (abbexa, abx226552), anti-SARS-CoV-2 M (Novus Biologicals,
571 NBP3-05698), rabbit anti-SARS-CoV-2 N (Novus Biologicals, NBP3-05730), mouse anti-FLAG
572 (CST, #2368), mouse anti-HIV-p24 (Abcam, ab9071) anti-Strep tag (IBA, 2-1507-001) and anti-
573 β-actin (CST, #4967). Membranes were washed with TBS-T and incubated with HRP-linked
574 secondary antibodies prior to detection with Clarity ECL chemiluminescence reagent (Bio-Rad).
575 All blots were imaged on a Bio-Rad ChemiDoc-Touch system. Molecular weights were
576 determined using the Broad Range, Color Prestained Protein Standard (NEB, P7719) or Precision
577 Plus Protein All Blue Prestained Protein Standards (BioRad, 1610373). Molecular weights in kDa
578 are indicated on the left of blot images. For quantitation of western blots, the total antibody signal
579 intensity was divided by the Stain-Free total protein signal. Images were analyzed using Image
580 Lab 6.1 (Bio-Rad). Images were cropped and annotated using Affinity Designer (Serif).
581
582 **Plasmid generation and transfections.** All plasmids were purified using the QIAprep Spin
583 Miniprep or QIAfilter Plasmid Midi Kits (QIAGEN) and all restriction enzymes were purchased
584 from New England Biolabs (NEB). The pcDNA3-SARS-CoV-2-Spike plasmid contains a codon-
585 optimized ORF for Spike from GenBank NC_045512 that was synthesized by GenScript (a kind
586 gift from David Kelvin) then cloned between the KpnI and BamHI sites of pcDNA3.1(+). A 19
587 residue C-terminal truncation of Spike (SΔ19) and Spike with a C-terminal FLAG tag was
588 generated by PCR. A Spike mutant lacking the Furin cleavage site between S1 and S2 (P681S,
589 R682G, R683G, R685del), and two-proline stabilizing mutants, K986P and V987P (S-2P) (70–
590 72) was generated by PCR mutagenesis using KOD Xtreme Hot Start DNA Polymerase (Sigma,
591 71975-M). pcDNA3-Membrane (M) and pcDNA3-Envelope (E) were cloned from pLVX-
592 EF1alpha-SARS-CoV-2-M-2xStrep-IRES-Puro and pLVX-EF1alpha-SARS-CoV-2-E-2xStrep-
593 IRES-Puro (kind gifts from Nevan Krogan, available from Addgene #141386 and #141385) using
594 PCR to remove the 2xStrep epitope tag. pCMV3-MERS-FLAG was purchased from
595 SinoBiologicals (VG40069-CF). pLJM1-Luc2 used in generating Spike-pseudotyped lentiviruses
596 was generated by cloning Luc2 from pGL4.26 (Promega) into pLJM1-B* (67). pLJM1-ACE2-
597 BSD was cloned by from cDNA of generated from Caco-2 cells. Primer sequences are listed in
598 Table 2. 293T cells were transfected using polyethylenimine (PEI; Linear, MW 25000
599 (Polysciences Inc., 23966) dissolved in water (pH 7.4). Both plasmids and PEI were diluted in
600 OptiMEM (Gibco), then combined for 15 min before adding to cell monolayers in serum-free

601 DMEM. PEI was used at 3:1 ratio to plasmid DNA. After 4 h, serum-free media was replaced with
602 DMEM containing 10% FBS with indicated treatments unless otherwise indicated. For pre-
603 treatments with ML099. the drug was applied at the time of transfection, then refreshed when the
604 media was changed 4 h after transfection. Generally, cells were lysed for immunoblotting analysis
605 at 24 h post-transfection (hpt). For flow-cytometry and immunofluorescence experiments, cells
606 were instead transfected with FugeneHD (Promega, E2311) according to the manufacturer's
607 instructions.
608

609 **siRNA knockdown experiments.** All siRNAs were obtained from Invitrogen. 293T cells (1-1.5
610 x 10^5 cells/mL) in 10% DMEM were reverse transfected with Lipofectamine RNAiMAX
611 (Invitrogen, 13778075) and 10 nM of Silencer Select negative siRNA #2 (4390846), HPRT1
612 siRNA #1 (s6889), or HPRT1 siRNA #2 (s6888) diluted in OptiMEM (Gibco, 31985070). RNA
613 was harvested from cells 48 hpt knockdown validation by RT-qPCR. For determining the effect
614 of HPRT1 knockdown on viral titer after 6-TG treatment, the reverse transfected cells were
615 infected at 24 hpt at an MOI of 0.1 then treated with DMSO or 10 µM 6-TG as described above.
616 After a 24 h infection, the cell supernatant for titration, and the infected monoloayers were lysed
617 with 2x Laemmli Buffer and processed for western blotting.

618

619 **Production of SARS-CoV-2 virus-like particles.** To generate SARS-CoV-2 virus-like particles,
620 293T cells were seeded in a 10 cm dish and co-transfected with 2 µg of each pcDNA-Spike,
621 pcDNA-M, pcDNA-E, and pLVX-EF1alpha-SARS-CoV-2-N-2xStrep-IRES-Puro (a kind gift
622 from Neven Krogan, available from Addgene #141391) with PEI, then treated with 6-TG or
623 DMSO as described above. After two days, supernatant was harvested and filtered through a 0.45
624 µm filter. For concentration and western blot analysis, filtered supernatant was underlaid with 20%
625 sucrose PBS using a pipetting needle and centrifuged at 39 000 rpm for 2 h using an SW-41 rotor
626 (Beckman Coulter). The supernatant and sucrose solution were carefully removed, and the pellet
627 was resuspended in PBS, mixed in equal proportions with 2x Laemmli Buffer with 100 mM DTT
628 and boiled at 95°C for 5 min before analysis by western blot.

629

630 **SARS-CoV-2 Spike-pseudotyped lentiviruses.** To generate Spike-pseudotyped lentivirus
631 particles, 293T cells were seeded in a 10 cm dish and co-transfected with 3 µg pLJM1-Luc2, 2 µg
632 pSPAX2 (a kind gift from Didier Trono; Addgene #12260), and 2 µg of pcDNA3- SΔ19 with PEI,
633 then treated with 6-TG or DMSO as described above. After two days, supernatant was harvested,
634 filtered through a 0.45 µm filter, aliquoted and stored at -80°C until use. Genomes were quantified
635 using a qPCR Lentivirus Titer Kit (Applied Biological Materials, LC900) as per the
636 manufacturer's instructions. Infectious pseudotyped particles were measured by infecting 293A
637 cells stably expressing ACE2 or an EV control. Cell lysates were harvested 24 h after infection in
638 Reporter Lysis Buffer (Promega, E397A), lysed by freeze thawing at -80°C, and luciferase activity
639 was measured using Luciferase Assay reagent (Promega) on a FLUOstar Omega microplate reader
640 (BMG Labtech). Lentiviruses that were concentrated and analyzed by western blot were prepared
641 as described above for SARS-CoV-2 virus-like particles.

642

643 **Transmission electron microscopy (TEM).** Samples were prepared and visualized as described
644 in (73). Briefly, HCoV-OC43 containing supernatant was concentrated by ultracentrifugation as
645 described above, fixed with 2.5% glutaraldehyde (Electron Microscopy Sciences) , then applied to
646 Formvar/carbon coated grids and left to settle to 10 min. The grid was then rinsed with distilled
647 water then stain with 2% w/v uranyl acetate for 30 s. Residual stain was wicked off with filter
648 paper then left to air dry completely. Grids were imaged on a JEM 1230 TEM (JEOL) running at
649 80 kV using an OCRA-HR camera (Hamamatsu). Sample preparation, fixation, and TEM imaging
650 were performed twice with representative images from one independent experiment shown.

651

652 **Quantitation of SARS-CoV-2 Spike surface expression.** 293T cells were co-transfected with
653 pEGFP-N1 and plasmids expressing SARS-CoV-2 Spike (FL) or SARS-CoV-2 Spike-Δ19 for 24
654 h using FugeneHD (Promega). The cells were treated with DMSO or 10 µM 6-TG at 4 h post-
655 transfection. At 24 h post-transfection, the cells were lifted with 10 mM EDTA PBS and pelleted
656 at 300 x *g* for 5 min. Cells were washed once with wash buffer (2 mM EDTA, 2% FBS, PBS),
657 then stained with 0.1 µg/sample Alexa Fluor 647-conjugated mouse-anti SARS-CoV-2 Spike S1
658 (R&D Systems, FAB105403R-100UG) at 4°C for 30 min in the dark. Cells were then washed prior
659 to fixation with 2% paraformaldehyde (Electron Microscopy Sciences) in PBS at 4°C for 30 min

660 in the dark, then washed and stored at 4°C in the dark until analysis using a FACSCelesta cell
661 analyzer (BD Biosciences) configured with 405 nm, 488 nm, and 640 nm lasers using the same
662 acquisition voltages for all replicates with at least 50000 single cells acquired per sample. The data
663 were analyzed using FCS Express v. 6.06.0040 (De Novo Software) where transfected single cells
664 were selected by EGFP fluorescence and analyzed for Spike surface expression via Alexa Fluor
665 647 fluorescence.

666

667 ***Gaussia* luciferase secretion assays.** For short-term treatments, 293T were transfected with
668 pCMV-*Gaussia* Luc Vector (ThermoFisher Scientific, 16147) as described above. After 18 h,
669 medium was removed and replaced with fresh medium containing 6-TG, BFA, or DMSO. After 6
670 h medium was removed, debris was cleared by centrifuging samples at 5,000 × *g* for 5 min, then
671 samples were stored at -80°C until measuring *Gaussia* luciferase activity using the *Gaussia*
672 Luciferase Flash Assay Kit (ThermoFisher Scientific, 16158) as per the manufacturer's directions
673 on a FLUOstar Omega microplate reader (BMG Labtech). For long-term treatments, 293T cells
674 were co-transfected with pCMV-*Gaussia* Luc and pLJM1-Luc2 and treated 6 h post transfection.
675 After 24 h, supernatant harvested as described above. The cell monolayer was lysed in Reporter
676 Lysis Buffer (Promega) as described above. To measure both Luciferase and *Gaussia* luciferase
677 activity in samples, we used the Dual-Luciferase Reporter Assay System (Promega, E1910), which
678 although designed for firefly and *Renilla* luciferase, can be readily adapted for firefly and *Gaussia*
679 luciferase as both *Gaussia* and *Renilla* luciferase both use coelenterazine as a substrate.

680

681 **Statistical analysis.** Statistical analysis and graphing were performed using GraphPad PRISM (v.8
682 or v.9). Statistically significant differences were determined using Dunnett's multiple comparison
683 test for one-way ANOVA and Šídák's multiple comparison test for two-way ANOVA.

684

685 **Graphics.** Molecular models were created with NCBI PubChem
686 (http://pubchem.ncbi.nlm.nih.gov/) The model presented in Fig. 7 was adapted from "Coronavirus
687 Replication Cycle", by BioRender.com (2022). Retrieved from
688 https://app.biorender.com/biorender-templates.

ACKNOWLEDGEMENTS

We are grateful for the support of the Dalhousie University Flow Cytometry Core Facility and the Cellular and Molecular Digital Imaging Core Facility. This work was supported by Canadian Institutes for Health Research (CIHR) Project Grant PJT-148727 (to C.M.), Natural Sciences and Engineering Research Council (NSERC) of Canada Discovery Grant RGPIN-2016-05083 (to S.L.B.), Coronavirus Variants Rapid Response Network (CoVaRR-Net) Grant 175622 (to J.A.C. and others), Research Nova Scotia Grant RNS-NHIG-2020-1383 and Lung Association of Nova Scotia Legacy Research Grant (to D.K.), and a Nova Scotia COVID-19 Health Research Coalition Grant to C.M. and E.S.P. SARS-CoV-2 research is supported in the laboratory of D.F. by the Canadian Institutes of Health Research (CIHR; OV5-170349, VRI-173022 and VS1-175531). VIDO receives operational funding from the Government of Saskatchewan through Innovation Saskatchewan and the Ministry of Agriculture and from the Canada Foundation for Innovation through the Major Science Initiatives for its CL3 facility.

CONFLICT OF INTEREST

E.S.P. is a consultant for Aegis Life Inc. All other authors declare no conflicts of interest.

708 **Table 1**. Primer sequences for RT-qPCR analysis

Target	Sequence (5′-3′)	
OC43 Orf1a	F – ATATGGCCAAGGCTGGTGAC	R – ATGTAACACGCCTTCCAGCA
OC43 S	F – TCTTCCGAACCAGCATTGCT	R – TAATGGGTTGCAGCTGTCGT
OC43 N	F – GGACCCAAGTAGCGATGAGG	R – GTGCGCGAAGTAGATCTGGA
18S	F – TTCGAACGTCTGCCCTATCAA	R – GATGTGGTAGCCGTTTCTCAGG
HPRT1	F – CGAGATGTGATGAAGGAGATG	R – GCAGGTCAGCAAAGAATTTATAG
Xbp1	F – TAGCAGCTCAGACTGCCAGA	R – CCAAGCGCTGTCTTAACTCC
ERdj4	F – CGCCAAATCAAGAAGGCCT	R – CAGCATCCGGGCTCTTATTTT
EDEM1	F – TTGACAAAGATTCCACCGTCC	R – TGTGAGCAGAAAGGAGGCTT
ATF3	F – AGGCGACGAGAAAGAAATAAG	R – TTCACACTTTCCAGCTTCTC
CHOP	F – ATGAACGGCTCAAGCAGGAA	R – GGGAAAGGTGGGTAGTGTGG
HERPUD1	F – AACGGCATGTTTTGCATCTG	R – GGGGAAGAAAGGTTCCGAAG
BiP	F – GCCTGTATTTCTAGACCTGCC	R – TTCATCTTGCCAGCCAGTTG

709

710 **Table 2.** Primers used for cloning and PCR mutagenesis

Gene	Sequence (5′-3′)
Spike	F - AATTGGTACCATGTTCGTCTTTCTGGTTCTGTTGCC
	R - AATTGGATCCTCAAGTGTAGTGCAGTTTCACGC
Spike-S0	F - CTCCGTGGCAAGCCAGTCGATCATCGCCTAC
	R - GCGCCTCCACTCGAGTTCGTCTGGGTCTGGTA
Spike-Flag	F - AATTGGTACCATGTTCGTCTTTCTGGTTCTGTTGCC
	R - AATTGGATCCTTACTTATCGTCGTCATCCTTGTAAT CAGAGCCTCCACCCCCAGTGTAGTGCAGTTTCACGC
Spike-Δ19	F - AATTGGTACCATGTTCGTCTTTCTGGTTCTGTTGCC

	R - AATTGGATCCTTAACAACAACTACCGCAACTGC
Spike-2P	F - CCGGAGGCCGAGGTGCAGATCGAC
	R - TGGGTCCAGTCTTGACAGGATGTCGTTC
E	F - AATTGCTAGCACCATGTACAGCTTCG
	R - AATTGAATTCTTAAACGAGGAGATCCGGCAC
M	F - AATTGCTAGCACCATGGCCGACTCAAATGG
	R - AATTGAATTCTTACTGGACGAGTAAAGC
ACE2	F - AATTACCGGTATGTCAAGCTCTTCCTGGC
	R - AATTGTCGACCTAAAAGGAGGTCTGAACATCATCAG

714 **FIGURE LEGENDS**

715 **Figure 1. Thiopurines 6-thioguanine and 6-thioguanosine inhibit coronavirus replication. (A)**
716 Structures of thiopurines used this study in comparison to guanine. **(B)** Calu-3 cells were infected
717 with SARS-CoV-2 at an MOI of 0.1 then treated with 6-thioguanine (6-TG), 6-thioguanosine (6-
718 TGo), or 6-mercaptopurine (6-MP). Supernatant was harvested after 48 h, and stored at -80∞C
719 until titering on Vero'76 cells. Mock-infected cells were similarly treated with 6-TG, 6-TGo, 6-
720 MP, or DMSO vehicle control for 48 h before testing cell viability with CellTiter 96 AQueous One
721 (n=3 ± SEM). Dotted line indicated Limit of Detection. **(C)** Summary table of 50% Cytoxic
722 Concentration (CC_{50}), 50% Effective Concentration (EC_{50}), and Selectivity Index (SI) calculated
723 for (A-C). **(D)** Alamar Blue cell viability assay of hTert-BJ, HCT-8, and Huh-7.5 cells treated with
724 6-TG (n=3±SEM). **(E)** TCID assays for HCoV-OC43 infected HCT-8 cells and **(F)** HCoV-229E
725 infected Huh-7.5. Cells were infected with an MOI of 0.1 then treated with 6-TG, 6-TGo, 6-MP,
726 or DMSO (n=3 ± SEM, statistical significance was determined by one-way ANOVA). **(F)** hTERT-
727 BJ cells were infected with HCoV-OC43 or HCoV-229E at an MOI of 0.1 and treated with 6-TG,
728 Tm, or DMSO. Supernatant was harvested after 23 h and stored at -80∞C before titering on BHK-
729 21 or Huh7.5 (n=3-4 ± SEM, statistical significance was determined by one-way ANOVA). **(G)**
730 hTERT-BJ cells were infected with HCoV-OC43 or **(H)** HCoV-229E at an MOI of 0.1 and treated
731 with 6-TG, Tm, or DMSO. Supernatant was harvested after 23 h and stored at -80∞C before
732 titering on BHK-21 or Huh7.5 (n=3-4 ± SEM, statistical significance was determined by one-way
733 ANOVA). LoD = Limit of Detection for virus titer. (*, $p<0.05$; **, $p<0.01$; ns, non-significant)

734 **Figure 2. 6-TG reduces CoV protein and mRNA accumulation. (A-C)** 293T cells were infected
735 with HCoV-OC43 at an MOI of 0.1 then treated with 10 μM 6-TG or DMSO vehicle control.
736 Supernatant and total RNA from the cells were harvested at the times indicated and stored at -

737 80∞C until **(A)** titering on BHK-21 or **(B)** quantification of viral genomes by RT-qPCR. Cell
738 monolayers were harvested for **(C)** RT-qPCR analysis of viral RNA accumulation (n=3 statistical
739 significance was determined by paired ratio t test; *, $p<0.05$; **, $p<0.01$; ns, non-significant).**(D)**
740 293T cells were infected as in (A) then treated with 5 or 10 μM 6-TG or DMSO. Lysates were
741 harvested 24h after infection and were probed by western blotting as indicated. **(E)** 293T cells
742 were grown on coverslips then infected with HCoV-OC43 and treated with 6-TG as in (A), then
743 fixed and immunostained for N or **(F)** dsRNA. Nuclei are counterstained with Hoechst. Scale bar
744 = 20 μm.

745

746 **Figure 3. 6-TG inhibits Spike glycosylation and cleavage. (A)** Calu-3 cells were infected with
747 SARS-CoV-2 at an MOI of 7, then treated with 6-TG or DMSO. Lysates were harvested 48 h after
748 infection and were probed by western blotting as indicated. Concentrations in legend are in μM.
749 **(B)** Huh-7.5 cells were infected with SARS-CoV-2 at an MOI of 5, then treated with 6-TG or
750 DMSO. Lysates were harvested 48 h after infection and were probed by western blotting as
751 indicated. Concentrations in legend are in μM. **(C)** 293T cells were transfected with SARS-CoV-
752 2 S, M, Envelope (E), Nucleoprotein (N) with a C-terminal 2xStrep tag, or EV then treated with
753 10 μM 6-TG or DMSO vehicle control. Lysates were harvested 24 h after transfection and probed
754 by western blotting as indicated. **(D)** 293T cells were transfected with SARS-CoV-2 Spike or EV
755 then treated with 6-TG or DMSO vehicle control. Lysates were harvested 24 h after transfection
756 and were probed by western blotting as indicated. Concentrations in legend are in μM. **(E)** Alamar
757 Blue cell viability assay of 6-TG treated 293T cells (n=3±SEM). **(F)** 293T cells were transfected
758 with SARS-CoV-2 Spike (S), a Spike mutant lacking the Furin cleavage site between S1 and S2
759 (S0), or EV then treated with 10 μM 6-TG or DMSO vehicle control. Lysates were harvested 24

760 h after transfection, treated with PNGase F to remove N-linked glycans, and probed by western
761 blotting as indicated. **(G)** as in (C) except 293T cells were transfected with C-terminal FLAG-
762 tagged Spike (S-FL) or HCoV-MERS Spike (MERS).

763

764 **Figure 4. 6-TG stimulates an assembly defect and inhibits Spike virion incorporation. (A)**
765 293T cells were transfected with equal quantities of SARS-CoV-2 S, M, E, and N plasmids or
766 empty vector (EV) then treated with 10 μM 6-TG or DMSO vehicle control. Lysates were
767 harvested 48 h after transfection and probed by western blotting as indicated. **(B)** Virus-like
768 particles from supernatants of cells transfected in (B) were concentrated by ultracentrifugation
769 through a 20% sucrose cushion, resuspended in PBS, then harvested with an equal volume of 2x
770 Laemmli buffer. Samples from two independent lentivirus preparations were probed by western
771 blotting as indicated. **(C)** 293T cells were transfected with S, E, M, and N in a 1:2:2:1 ratio,
772 substituting one of the structural proteins for EV as indicated, treated with 6-TG or DMSO then
773 processed as in (A). **(D)** SARS-CoV-2 Spike pseudotyped, luciferase-expressing lentivirus
774 particles were concentrated by ultracentrifugation through a 20% sucrose cushion, resuspended in
775 PBS, then harvested with an equal volume of 2x Laemmli buffer. Samples from three independent
776 lentivirus preparations were probed by western blotting as indicated. **(E)** Genomes from three
777 independent lentivirus preparations were quantified by RT-qPCR (n=3, statistical significance was
778 determined by paired t-test; ns, non-significant). **(F)** 293A cells stably expressing ACE2 or empty
779 vector control were transduced with lentivirus from three independent preparations. After 24 h,
780 lysates were harvested and measured for luciferase activity (n=3, statistical significance was
781 determined by two-way ANOVA; *, $p<0.05$; ns, non-significant). **(G)** 293A cells were infected
782 HCoV-OC43 at an MOI of 0.1 =, then treated with 6-TG or DMSO. Supernatants were

783 concentrated as in (C), before virions were fixed and imaged by TEM with negative staining. Five
784 virions from both 6-TG- and DMSO-treated samples are shown at 150,000 X magnification. Scale
785 bar = 100 nm. Arrowhead indicates examples of Spike protein extending from virion.

786

787 **Figure 5. 6-TG inhibits Spike maturation through GTPase inhibition. (A)** 6-TG is conjugated
788 to phosphoribosyl diphosphate (PRPP) by HPRT1 to form 6-TG monophosphate. 6-TG methylated
789 at the N9 nitrogen was designed to be resistant to processing by HPRT1. **(B)** 293T cells were
790 infected with HCoV-OC43 at an MOI of 0.1 then treated with 6-TG or 6-TG-Me. Supernatant was
791 harvested at 24 hpi and stored at -80∞C until titering on BHK cells. (n=3 statistical significance
792 was determined by paired ratio t test; *, $p<0.05$; **, $p<0.01$; ns, non-significant). **(C)** 293T cells
793 were transfected with SARS-CoV-2 Spike or an empty vector control then treated with 6-TG, 6-
794 TG-Me, or DMSO vehicle control. Lysates were harvested 24 h after transfection and probed by
795 western blotting as indicated. **(D)** 293T cells were reversed transfected with siRNA and total RNA
796 was harvested after 48 h. HPRT1mRNA abundance was measured by RT-qPCR (n=3, ±SEM
797 statistical significance was determined by one way ANOVA; ***, $p<0.001$). **(E)** As in D but cells
798 were infected with HCoV-OC43 at an MOI of 0.1 24 h after siRNA treatment and supernatant was
799 harvested and titered as in **(B)** (n=4 ±SEM statistical significance was determined by paired ratio
800 t test; **, $p<0.01$; ***, $p<0.001$; ns, non-significant).

801

802 **Figure 6. 6-TG inhibits Spike maturation through GTPase inhibition. (A)** alamarBlue cell
803 viability assay of 293T cells treated Rac1 Inhibitor V (Rac1iV), Rhosin, CASIN, or ML099
804 (n=3±SEM). **(B)** Summary table of 50% Cytotoxic concentration (CC_{50}) and inhibitor target of

805 compounds tested in (A). **(C)** 293T cells were transfected with SARS-CoV-2 Spike or an empty
806 vector control (EV) then treated with 6-TG, GTPase inhibitors, or DMSO vehicle control.
807 Concentrations in legend are in μM. Lysates were harvested 24 h after transfection and were
808 probed by western blotting as indicated. **(D)** 293T cells were transfected with plasmids encoding
809 Spike or EV then co-treated with 6-TG, 100 μM ML099 GTPase agonist, or DMSO. Lysates were
810 harvested 24 h after transfection and were probed by western blotting as indicated. Concentrations
811 in legend are in μM. **(E)** as in (D) except some samples were pre-treated (Pre) for 4 h with ML099.
812 **(F)** HCT-8 and 293A were infected with an MOI of ~0.1 then treated with 10 μM 6-TG or DMSO
813 vehicle control. After 24 h, the supernatants were harvested and stored at -80ºC until titering on
814 BHK-21 (n=3 ± SEM, statistical significance was determined by one-way ANOVA; *, $p<0.05$;
815 **, $p<0.01$; ns, non-significant). LoD = Limit of Detection for virus titer.

816

817 **Figure 7. 6-TG inhibits multiple essential steps in virus replication and assembly.** 6-TG
818 inhibits nsp3/papain-like protease (PLpro), delaying formation of replication compartments and
819 reducing accumulation of viral RNA. 6-TG also inhibits normal glycosylation of Spike, which fails
820 to be properly packaged in egressing virions. As a result, the total number of virions released from
821 infected cells is reduced and those that are released have fewer Spikes on their surface.

822

823 **Figure S1. Activation of the unfolded protein response (UPR) during OC43 infection. (A)**
824 293T cells were infected with HCoV-OC43 at an MOI of 0.1 then treated with 10 μM 6-TG or
825 DMSO vehicle control. Total RNA from the cells were harvested at the times indicated and stored
826 at -80∞C until RT-qPCR analysis of UPR target genes. **(B)** 293A cells were infected as in (A),

827 then treated with 10 µg 6-TG, 1µg thapsigargin (Tg), or DMSO. Cells were treated with 10 µg/mL
828 of puromycin for 10 min prior to harvest 24 h after infection. Lysates were probed by western blot
829 as indicated. **(C)** Total puromycin intensity from (E) was quantified relative to total protein load
830 and are graphed normalized to the mock-infected, DMSO-treated cells (n=3 ± SEM, statistical
831 significance was determined by paired t-test compared to mock-infected, DMSO-treated cells; *,
832 p<0.05; **, p<0.01; ***, p<0.001; ns, non-significant).

833

834 **Figure S2. 6-TG reduces surface expression of Spike but does not globally limit secretion.**
835 **(A)** alamarBlue cell viability assay of 293T cells treated with brefeldin A (BFA) (n=4±SEM). **(B)**
836 293T cells were transfected with *Gaussia* luciferase for 18 h then treated with 6-TG, BFA or
837 DMSO vehicle control for 6 h. Supernatants were recovered from the cells and measured for
838 luciferase activity. **(C)** 293T cells were transfected with both luciferase and *Gaussia* luciferase
839 then treated with 6-TG, BFA, or DMSO. After 24 h, supernatants were removed and analyzed as
840 in (B). Cell lysate was harvested in Reporter Lysis Buffer and stored at -80∞C until both luciferase
841 and *Gaussia* luciferase activity was measured. (For B and C, n=3 ± SEM, statistical significance
842 was determined by paired t-test compared to DMSO-treated cells; *, p<0.05; **, p<0.01; ***,
843 p<0.001; ns, non-significant). **(D)** 293T cells were transfected with SARS-CoV-2 Spike or EV
844 then treated with 6-TG, BFA, or DMSO. Lysates were harvested 24 h after transfection in 2x
845 Laemmli buffer and were probed by western blotting as indicated. **(E)** 293T cells were co-
846 transfected with EGFP and either Spike (S), Spike with 19 residue C-terminal truncation (SΔ19),
847 or EV and then treated with 10 µM 6-TG or DMSO. After 24 h, cells were harvested, surface-
848 stained for Spike then fixed prior to analysis by flow cytometry. EGFP+ cells were gated for

849 analysis of number of Spike+ cells and Median Fluorescent Intensity (MFI) (n=4±SEM statistical

850 significance was determined by paired t-test between 6-TG and DMSO treated cells; *, $p<0.05$).

851

852 **REFERENCES**

853 1. Angelini MM, Akhlaghpour M, Neuman BW, Buchmeier MJ. 2013. Severe acute
854 respiratory syndrome coronavirus nonstructural proteins 3, 4, and 6 induce double-
855 membrane vesicles. mBio 4:e00524-13.

856 2. Gosert R, Kanjanahaluethai A, Egger D, Bienz K, Baker SC. 2002. RNA replication of
857 mouse hepatitis virus takes place at double-membrane vesicles. J Virol 76:3697–3708.

858 3. Knoops K, Kikkert M, Worm SHE van den, Zevenhoven-Dobbe JC, van der Meer Y,
859 Koster AJ, Mommaas AM, Snijder EJ. 2008. SARS-coronavirus replication is supported by
860 a reticulovesicular network of modified endoplasmic reticulum. PLoS Biol 6:e226.

861 4. Beachboard DC, Anderson-Daniels JM, Denison MR. 2015. Mutations across murine
862 hepatitis virus nsp4 alter virus fitness and membrane modifications. J Virol 89:2080–2089.

863 5. Oudshoorn D, Rijs K, Limpens RWAL, Groen K, Koster AJ, Snijder EJ, Kikkert M,
864 Bárcena M. 2017. Expression and Cleavage of Middle East Respiratory Syndrome
865 Coronavirus nsp3-4 Polyprotein Induce the Formation of Double-Membrane Vesicles That
866 Mimic Those Associated with Coronaviral RNA Replication. mBio 8:e01658-17.

867 6. Doyle N, Hawes PC, Simpson J, Adams LH, Maier HJ. 2019. The Porcine
868 Deltacoronavirus Replication Organelle Comprises Double-Membrane Vesicles and
869 Zippered Endoplasmic Reticulum with Double-Membrane Spherules. Viruses 11:E1030.

870 7. Snijder EJ, Limpens RWAL, de Wilde AH, de Jong AWM, Zevenhoven-Dobbe JC, Maier
871 HJ, Faas FFGA, Koster AJ, Bárcena M. 2020. A unifying structural and functional model

872 of the coronavirus replication organelle: Tracking down RNA synthesis. PLoS Biol
873 18:e3000715.

874 8. Wolff G, Limpens RWAL, Zevenhoven-Dobbe JC, Laugks U, Zheng S, de Jong AWM,
875 Koning RI, Agard DA, Grünewald K, Koster AJ, Snijder EJ, Bárcena M. 2020. A
876 molecular pore spans the double membrane of the coronavirus replication organelle.
877 Science 369:1395–1398.

878 9. Kanjanahaluethai A, Chen Z, Jukneliene D, Baker SC. 2007. Membrane topology of murine
879 coronavirus replicase nonstructural protein 3. Virology 361:391–401.

880 10. Oostra M, te Lintelo EG, Deijs M, Verheije MH, Rottier PJM, de Haan C a. M. 2007.
881 Localization and membrane topology of coronavirus nonstructural protein 4: involvement
882 of the early secretory pathway in replication. J Virol 81:12323–12336.

883 11. Tooze J, Tooze S, Warren G. 1984. Replication of coronavirus MHV-A59 in sac- cells:
884 determination of the first site of budding of progeny virions. Eur J Cell Biol 33:281–293.

885 12. Goldsmith CS, Tatti KM, Ksiazek TG, Rollin PE, Comer JA, Lee WW, Rota PA, Bankamp
886 B, Bellini WJ, Zaki SR. 2004. Ultrastructural characterization of SARS coronavirus. Emerg
887 Infect Dis 10:320–326.

888 13. Stertz S, Reichelt M, Spiegel M, Kuri T, Martínez-Sobrido L, García-Sastre A, Weber F,
889 Kochs G. 2007. The intracellular sites of early replication and budding of SARS-
890 coronavirus. Virology 361:304–315.

891 14. Ghosh S, Dellibovi-Ragheb TA, Kerviel A, Pak E, Qiu Q, Fisher M, Takvorian PM, Bleck
892 C, Hsu VW, Fehr AR, Perlman S, Achar SR, Straus MR, Whittaker GR, de Haan CAM,
893 Kehrl J, Altan-Bonnet G, Altan-Bonnet N. 2020. β-Coronaviruses Use Lysosomes for
894 Egress Instead of the Biosynthetic Secretory Pathway. Cell 183:1520-1535.e14.

895 15. Fung TS, Liu DX. 2018. Post-translational modifications of coronavirus proteins: roles and
896 function. Future Virol 13:405–430.

897 16. Delmas B, Laude H. 1990. Assembly of coronavirus spike protein into trimers and its role
898 in epitope expression. J Virol 64:5367–5375.

899 17. Belouzard S, Chu VC, Whittaker GR. 2009. Activation of the SARS coronavirus spike
900 protein via sequential proteolytic cleavage at two distinct sites. Proc Natl Acad Sci U S A
901 106:5871–5876.

902 18. Millet JK, Whittaker GR. 2014. Host cell entry of Middle East respiratory syndrome
903 coronavirus after two-step, furin-mediated activation of the spike protein. Proc Natl Acad
904 Sci U S A 111:15214–15219.

905 19. Boson B, Legros V, Zhou B, Siret E, Mathieu C, Cosset F-L, Lavillette D, Denolly S. 2021.
906 The SARS-CoV-2 envelope and membrane proteins modulate maturation and retention of
907 the spike protein, allowing assembly of virus-like particles. J Biol Chem 296:100111.

908 20. Schoeman D, Fielding BC. 2019. Coronavirus envelope protein: current knowledge. Virol J
909 16:69.

910 21. Liao Y, Fung TS, Huang M, Fang SG, Zhong Y, Liu DX. 2013. Upregulation of
911 CHOP/GADD153 during coronavirus infectious bronchitis virus infection modulates
912 apoptosis by restricting activation of the extracellular signal-regulated kinase pathway. J
913 Virol 87:8124–8134.

914 22. Fung TS, Liao Y, Liu DX. 2014. The endoplasmic reticulum stress sensor IRE1α protects
915 cells from apoptosis induced by the coronavirus infectious bronchitis virus. J Virol
916 88:12752–12764.

917 23. Versteeg GA, van de Nes PS, Bredenbeek PJ, Spaan WJM. 2007. The coronavirus spike
918 protein induces endoplasmic reticulum stress and upregulation of intracellular chemokine
919 mRNA concentrations. J Virol 81:10981–10990.

920 24. Xue M, Fu F, Ma Y, Zhang X, Li L, Feng L, Liu P. 2018. The PERK Arm of the Unfolded
921 Protein Response Negatively Regulates Transmissible Gastroenteritis Virus Replication by
922 Suppressing Protein Translation and Promoting Type I Interferon Production. J Virol
923 92:e00431-18.

924 25. Favreau DJ, Desforges M, St-Jean JR, Talbot PJ. 2009. A human coronavirus OC43 variant
925 harboring persistence-associated mutations in the S glycoprotein differentially induces the
926 unfolded protein response in human neurons as compared to wild-type virus. Virology
927 395:255–267.

928 26. Tang BSF, Chan K-H, Cheng VCC, Woo PCY, Lau SKP, Lam CCK, Chan T-L, Wu AKL,
929 Hung IFN, Leung S-Y, Yuen K-Y. 2005. Comparative host gene transcription by

930 microarray analysis early after infection of the Huh7 cell line by severe acute respiratory
931 syndrome coronavirus and human coronavirus 229E. J Virol 79:6180–6193.

932 27. Chan C-P, Siu K-L, Chin K-T, Yuen K-Y, Zheng B, Jin D-Y. 2006. Modulation of the
933 unfolded protein response by the severe acute respiratory syndrome coronavirus spike
934 protein. J Virol 80:9279–9287.

935 28. Yeung Y-S, Yip C-W, Hon C-C, Chow KYC, Ma ICM, Zeng F, Leung FCC. 2008.
936 Transcriptional profiling of Vero E6 cells over-expressing SARS-CoV S2 subunit: insights
937 on viral regulation of apoptosis and proliferation. Virology 371:32–43.

938 29. Bechill J, Chen Z, Brewer JW, Baker SC. 2008. Coronavirus infection modulates the
939 unfolded protein response and mediates sustained translational repression. J Virol 82:4492–
940 4501.

941 30. Siu K-L, Chan C-P, Kok K-H, Woo PC-Y, Jin D-Y. 2014. Comparative analysis of the
942 activation of unfolded protein response by spike proteins of severe acute respiratory
943 syndrome coronavirus and human coronavirus HKU1. Cell Biosci 4:3.

944 31. Ye Z, Wong CK, Li P, Xie Y. 2008. A SARS-CoV protein, ORF-6, induces caspase-3
945 mediated, ER stress and JNK-dependent apoptosis. Biochim Biophys Acta 1780:1383–
946 1387.

947 32. Minakshi R, Padhan K, Rani M, Khan N, Ahmad F, Jameel S. 2009. The SARS
948 Coronavirus 3a protein causes endoplasmic reticulum stress and induces ligand-
949 independent downregulation of the type 1 interferon receptor. PloS One 4:e8342.

950 33. Sung S-C, Chao C-Y, Jeng K-S, Yang J-Y, Lai MMC. 2009. The 8ab protein of SARS-
951 CoV is a luminal ER membrane-associated protein and induces the activation of ATF6.
952 Virology 387:402–413.

953 34. Slaine PD, Kleer M, Duguay BA, Pringle ES, Kadijk E, Ying S, Balgi A, Roberge M,
954 McCormick C, Khaperskyy DA. 2021. Thiopurines activate an antiviral unfolded protein
955 response that blocks influenza A virus glycoprotein accumulation. J Virol JVI.00453-21.

956 35. Lepage GA. 1960. Incorporation of 6-thioguanine into nucleic acids. Cancer Res 20:403–
957 408.

958 36. Brem R, Karran P. 2012. Oxidation-mediated DNA cross-linking contributes to the toxicity
959 of 6-thioguanine in human cells. Cancer Res 72:4787–4795.

960 37. Shin J-Y, Wey M, Umutesi HG, Sun X, Simecka J, Heo J. 2016. Thiopurine Prodrugs
961 Mediate Immunosuppressive Effects by Interfering with Rac1 Protein Function. J Biol
962 Chem 291:13699–13714.

963 38. de Boer NKH, van Bodegraven AA, Jharap B, de Graaf P, Mulder CJJ. 2007. Drug Insight:
964 pharmacology and toxicity of thiopurine therapy in patients with IBD. Nat Clin Pract
965 Gastroenterol Hepatol 4:686–694.

966 39. Chou C-Y, Chien C-H, Han Y-S, Prebanda MT, Hsieh H-P, Turk B, Chang G-G, Chen X.
967 2008. Thiopurine analogues inhibit papain-like protease of severe acute respiratory
968 syndrome coronavirus. Biochem Pharmacol 75:1601–1609.

969 40. Chen X, Chou C-Y, Chang G-G. 2009. Thiopurine analogue inhibitors of severe acute
970 respiratory syndrome-coronavirus papain-like protease, a deubiquitinating and
971 deISGylating enzyme. Antivir Chem Chemother 19:151–156.

972 41. Cheng K-W, Cheng S-C, Chen W-Y, Lin M-H, Chuang S-J, Cheng I-H, Sun C-Y, Chou C-
973 Y. 2015. Thiopurine analogs and mycophenolic acid synergistically inhibit the papain-like
974 protease of Middle East respiratory syndrome coronavirus. Antiviral Res 115:9–16.

975 42. Swaim CD, Perng Y-C, Zhao X, Canadeo LA, Harastani HH, Darling TL, Boon ACM,
976 Lenschow DJ, Huibregtse JM. 2020. 6-Thioguanine blocks SARS-CoV-2 replication by
977 inhibition of PLpro protease activities. BioRxiv Prepr Serv Biol 2020.07.01.183020.

978 43. Tiede I, Fritz G, Strand S, Poppe D, Dvorsky R, Strand D, Lehr HA, Wirtz S, Becker C,
979 Atreya R, Mudter J, Hildner K, Bartsch B, Holtmann M, Blumberg R, Walczak H, Iven H,
980 Galle PR, Ahmadian MR, Neurath MF. 2003. CD28-dependent Rac1 activation is the
981 molecular target of azathioprine in primary human CD4+ T lymphocytes. J Clin Invest
982 111:1133–1145.

983 44. Poppe D, Tiede I, Fritz G, Becker C, Bartsch B, Wirtz S, Strand D, Tanaka S, Galle PR,
984 Bustelo XR, Neurath MF. 2006. Azathioprine suppresses ezrin-radixin-moesin-dependent T
985 cell-APC conjugation through inhibition of Vav guanosine exchange activity on Rac
986 proteins. J Immunol Baltim Md 1950 176:640–651.

987 45. Schultz DC, Johnson RM, Ayyanathan K, Miller J, Whig K, Kamalia B, Dittmar M,
988 Weston S, Hammond HL, Dillen C, Ardanuy J, Taylor L, Lee JS, Li M, Lee E, Shoffler C,
989 Petucci C, Constant S, Ferrer M, Thaiss CA, Frieman MB, Cherry S. 2022. Pyrimidine

990 inhibitors synergize with nucleoside analogues to block SARS-CoV-2. Nature
991 https://doi.org/10.1038/s41586-022-04482-x.

992 46. Al-Beltagi S, Preda CA, Goulding LV, James J, Pu J, Skinner P, Jiang Z, Wang BL, Yang
993 J, Banyard AC, Mellits KH, Gershkovich P, Hayes CJ, Nguyen-Van-Tam J, Brown IH, Liu
994 J, Chang K-C. 2021. Thapsigargin Is a Broad-Spectrum Inhibitor of Major Human
995 Respiratory Viruses: Coronavirus, Respiratory Syncytial Virus and Influenza A Virus.
996 Viruses 13:234.

997 47. Al-Beltagi S, Goulding LV, Chang DKE, Mellits KH, Hayes CJ, Gershkovich P, Coleman
998 CM, Chang K-C. 2021. Emergent SARS-CoV-2 variants: comparative replication dynamics
999 and high sensitivity to thapsigargin. Virulence 12:2946–2956.

1000 48. Shaban MS, Müller C, Mayr-Buro C, Weiser H, Meier-Soelch J, Albert BV, Weber A,
1001 Linne U, Hain T, Babayev I, Karl N, Hofmann N, Becker S, Herold S, Schmitz ML,
1002 Ziebuhr J, Kracht M. 2021. Multi-level inhibition of coronavirus replication by chemical
1003 ER stress. Nat Commun 12:5536.

1004 49. Santos-Beneit F, Raškevičius V, Skeberdis VA, Bordel S. 2021. A metabolic modeling
1005 approach reveals promising therapeutic targets and antiviral drugs to combat COVID-19.
1006 Sci Rep 11:11982.

1007 50. Oostra M, de Haan C a. M, de Groot RJ, Rottier PJM. 2006. Glycosylation of the severe
1008 acute respiratory syndrome coronavirus triple-spanning membrane proteins 3a and M. J
1009 Virol 80:2326–2336.

1010 51. Tarentino AL, Trimble RB, Plummer TH. 1989. Enzymatic approaches for studying the
1011 structure, synthesis, and processing of glycoproteins. Methods Cell Biol 32:111–139.

1012 52. Tian W, Li D, Zhang N, Bai G, Yuan K, Xiao H, Gao F, Chen Y, Wong CCL, Gao GF.
1013 2021. O-glycosylation pattern of the SARS-CoV-2 spike protein reveals an "O-Follow-N"
1014 rule. Cell Res https://doi.org/10.1038/s41422-021-00545-2.

1015 53. Sanda M, Morrison L, Goldman R. 2021. N- and O-Glycosylation of the SARS-CoV-2
1016 Spike Protein. Anal Chem 93:2003–2009.

1017 54. Shajahan A, Supekar NT, Gleinich AS, Azadi P. 2020. Deducing the N- and O-
1018 glycosylation profile of the spike protein of novel coronavirus SARS-CoV-2. Glycobiology
1019 30:981–988.

1020 55. Tannous BA, Kim D-E, Fernandez JL, Weissleder R, Breakefield XO. 2005. Codon-
1021 optimized Gaussia luciferase cDNA for mammalian gene expression in culture and in vivo.
1022 Mol Ther J Am Soc Gene Ther 11:435–443.

1023 56. Helms JB, Rothman JE. 1992. Inhibition by brefeldin A of a Golgi membrane enzyme that
1024 catalyses exchange of guanine nucleotide bound to ARF. Nature 360:352–354.

1025 57. Donaldson JG, Finazzi D, Klausner RD. 1992. Brefeldin A inhibits Golgi membrane-
1026 catalysed exchange of guanine nucleotide onto ARF protein. Nature 360:350–352.

1027 58. Crawford KHD, Eguia R, Dingens AS, Loes AN, Malone KD, Wolf CR, Chu HY, Tortorici
1028 MA, Veesler D, Murphy M, Pettie D, King NP, Balazs AB, Bloom JD. 2020. Protocol and

1029 Reagents for Pseudotyping Lentiviral Particles with SARS-CoV-2 Spike Protein for
1030 Neutralization Assays. Viruses 12:E513.

1031 59. Hu J, Gao Q, He C, Huang A, Tang N, Wang K. 2020. Development of cell-based
1032 pseudovirus entry assay to identify potential viral entry inhibitors and neutralizing
1033 antibodies against SARS-CoV-2. Genes Dis 7:551–557.

1034 60. Ou X, Liu Y, Lei X, Li P, Mi D, Ren L, Guo L, Guo R, Chen T, Hu J, Xiang Z, Mu Z, Chen
1035 X, Chen J, Hu K, Jin Q, Wang J, Qian Z. 2020. Characterization of spike glycoprotein of
1036 SARS-CoV-2 on virus entry and its immune cross-reactivity with SARS-CoV. Nat
1037 Commun 11:1620.

1038 61. Ujike M, Taguchi F. 2015. Incorporation of spike and membrane glycoproteins into
1039 coronavirus virions. Viruses 7:1700–1725.

1040 62. Nie J, Li Q, Wu J, Zhao C, Hao H, Liu H, Zhang L, Nie L, Qin H, Wang M, Lu Q, Li X,
1041 Sun Q, Liu J, Fan C, Huang W, Xu M, Wang Y. 2020. Establishment and validation of a
1042 pseudovirus neutralization assay for SARS-CoV-2. Emerg Microbes Infect 9:680–686.

1043 63. Schmidt F, Weisblum Y, Muecksch F, Hoffmann H-H, Michailidis E, Lorenzi JCC,
1044 Mendoza P, Rutkowska M, Bednarski E, Gaebler C, Agudelo M, Cho A, Wang Z,
1045 Gazumyan A, Cipolla M, Caskey M, Robbiani DF, Nussenzweig MC, Rice CM,
1046 Hatziioannou T, Bieniasz PD. 2020. Measuring SARS-CoV-2 neutralizing antibody activity
1047 using pseudotyped and chimeric viruses. J Exp Med 217:e20201181.

1048 64. Yin Y, Chen S, Hakim MS, Wang W, Xu L, Dang W, Qu C, Verhaar AP, Su J, Fuhler GM,
1049 Peppelenbosch MP, Pan Q. 2018. 6-Thioguanine inhibits rotavirus replication through
1050 suppression of Rac1 GDP/GTP cycling. Antiviral Res 156:92–101.

1051 65. Palsuledesai CC, Surviladze Z, Waller A, Miscioscia TF, Guo Y, Wu Y, Strouse J, Romero
1052 E, Salas VM, Curpan R, Young S, Carter M, Foutz T, Galochkina Z, Ames H, Haynes MK,
1053 Edwards BS, Nicolotti O, Luo L, Ursu O, Bologa CG, Oprea TI, Wandinger-Ness A, Sklar
1054 LA. 2018. Activation of Rho Family GTPases by Small Molecules. ACS Chem Biol
1055 13:1514–1524.

1056 66. Blight KJ, McKeating JA, Rice CM. 2002. Highly permissive cell lines for subgenomic and
1057 genomic hepatitis C virus RNA replication. J Virol 76:13001–13014.

1058 67. Johnston BP, Pringle ES, McCormick C. 2019. KSHV activates unfolded protein response
1059 sensors but suppresses downstream transcriptional responses to support lytic replication.
1060 PLoS Pathog 15:e1008185.

1061 68. Mendoza EJ, Manguiat K, Wood H, Drebot M. 2020. Two Detailed Plaque Assay Protocols
1062 for the Quantification of Infectious SARS-CoV-2. Curr Protoc Microbiol 57:ecpmc105.

1063 69. Craig N, Fletcher SL, Daniels A, Newman C, O'Shea M, Tan WS, Warr A, Tait-Burkard C.
1064 2022. Direct Lysis RT-qPCR of SARS-CoV-2 in Cell Culture Supernatant Allows for Fast
1065 and Accurate Quantification. Viruses 14:508.

1066 70. Wrapp D, Wang N, Corbett KS, Goldsmith JA, Hsieh C-L, Abiona O, Graham BS,
1067 McLellan JS. 2020. Cryo-EM structure of the 2019-nCoV spike in the prefusion
1068 conformation. Science 367:1260–1263.

1069 71. Pallesen J, Wang N, Corbett KS, Wrapp D, Kirchdoerfer RN, Turner HL, Cottrell CA,
1070 Becker MM, Wang L, Shi W, Kong W-P, Andres EL, Kettenbach AN, Denison MR,
1071 Chappell JD, Graham BS, Ward AB, McLellan JS. 2017. Immunogenicity and structures of
1072 a rationally designed prefusion MERS-CoV spike antigen. Proc Natl Acad Sci U S A
1073 114:E7348–E7357.

1074 72. Kirchdoerfer RN, Wang N, Pallesen J, Wrapp D, Turner HL, Cottrell CA, Corbett KS,
1075 Graham BS, McLellan JS, Ward AB. 2018. Stabilized coronavirus spikes are resistant to
1076 conformational changes induced by receptor recognition or proteolysis. Sci Rep 8:15701.

1077 73. Duguay BA, Herod A, Pringle ES, Monro SMA, Hetu M, Cameron CG, McFarland SA,
1078 McCormick C. 2022. Photodynamic Inactivation of Human Coronaviruses. Viruses 14:110.

1079

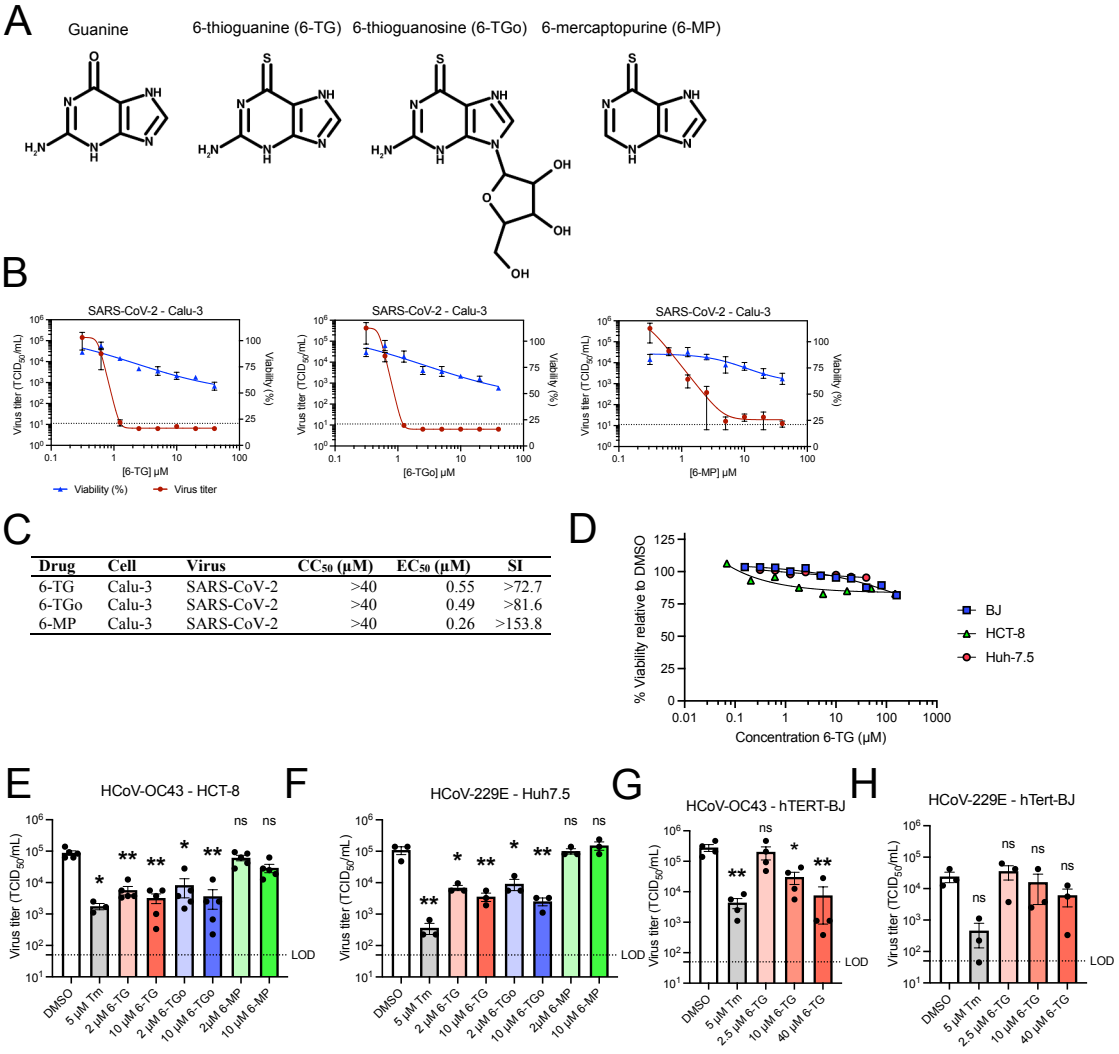

Drug	Cell	Virus	CC_{50} (µM)	EC_{50} (µM)	SI
6-TG	Calu-3	SARS-CoV-2	>40	0.55	>72.7
6-TGo	Calu-3	SARS-CoV-2	>40	0.49	>81.6
6-MP	Calu-3	SARS-CoV-2	>40	0.26	>153.8

Figure 1. Thiopurines 6-thioguanine and 6-thioguanosine inhibit coronavirus replication. (A) Structures of thiopurines used this study in comparison to guanine. **(B)** Calu-3 cells were infected with SARS-CoV-2 at an MOI of 0.1 then treated with 6-thioguanine (6-TG), 6-thioguanosine (6-TGo), or 6-mercaptopurine (6-MP). Supernatant was harvested after 48 h, and stored at -80°C until titering on Vero'76 cells. Mock-infected cells were similarly treated with 6-TG, 6-TGo, 6-MP, or DMSO vehicle control for 48 h before testing cell viability with CellTiter 96 AQueous One (n=3 ± SEM). Dotted line indicated Limit of Detection. **(C)** Summary table of 50% Cytoxic Concentration (CC_{50}), 50% Effective Concentration (EC_{50}), and Selectivity Index (SI) calculated for (A-C). **(D)** Alamar Blue cell viability assay of hTert-BJ, HCT-8, and Huh-7.5 cells treated with 6-TG (n=3±SEM).**(E)** TCID assays for HCoV-OC43 infected HCT-8 cells and **(F)** HCoV-229E infected Huh-7.5. Cells were infected with an MOI of 0.1 then treated with 6-TG, 6-TGo, 6-MP, or DMSO (n=3 ± SEM, statistical significance was determined by one-way ANOVA). **(F)** hTERT-BJ cells were infected with HCoV-OC43 or HCoV-229E at an MOI of 0.1 and treated with 6-TG, Tm, or DMSO. Supernatant was harvested after 23 h and stored at -80°C before titering on BHK-21 or Huh7.5 (n=3-4 ± SEM, statistical significance was determined by one-way ANOVA). **(G)** hTERT-BJ cells were infected with HCoV-OC43 or **(H)** HCoV-229E at an MOI of 0.1 and treated with 6-TG, Tm, or DMSO. Supernatant was harvested after 23 h and stored at -80°C before titering on BHK-21 or Huh7.5 (n=3-4 ± SEM, statistical significance was determined by one-way ANOVA). LoD = Limit of Detection for virus titer. (*, $p<0.05$; **, $p<0.01$; ns, non-significant)

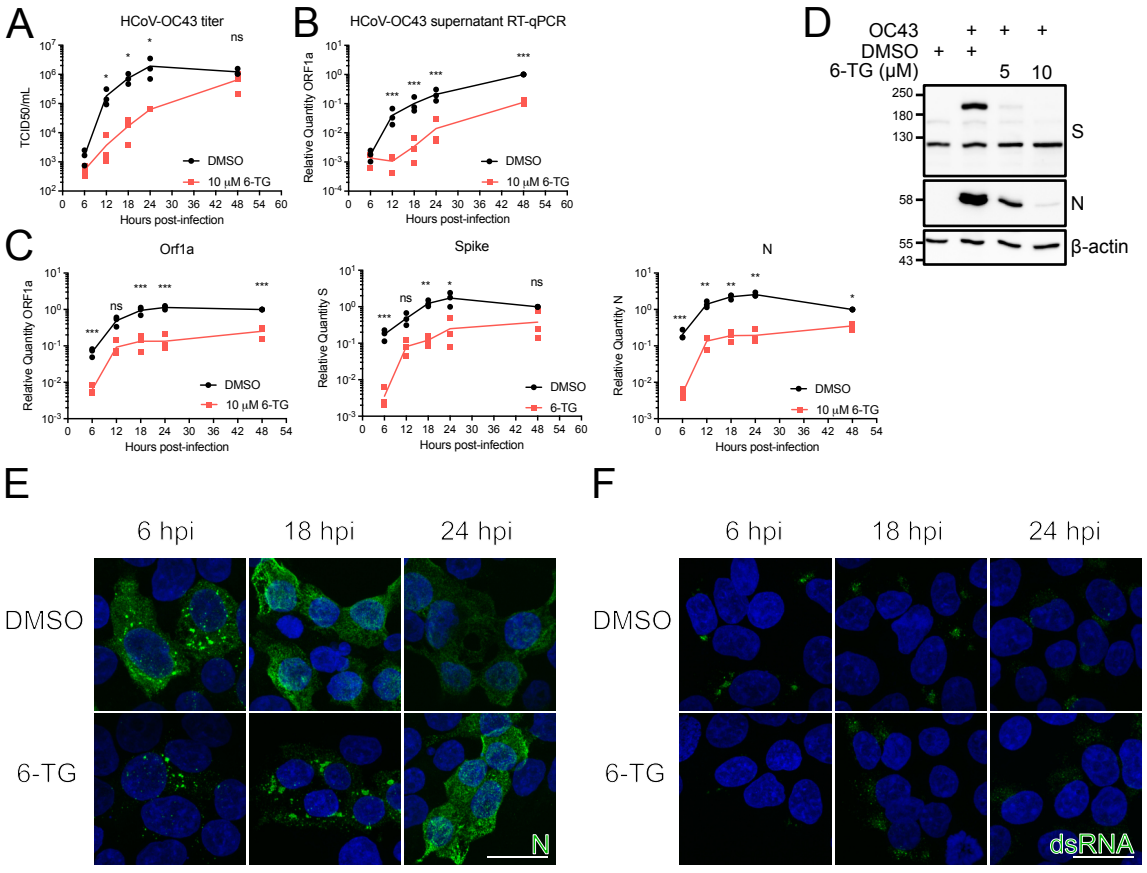

Figure 2. 6-TG reduces CoV protein and mRNA accumulation. (A-C) 293T cells were infected with HCoV-OC43 at an MOI of 0.1 then treated with 10 µM 6-TG or DMSO vehicle control. Supernatant and total RNA from the cells were harvested at the times indicated and stored at -80°C until **(A)** titering on BHK-21 or **(B)** quantification of viral genomes by RT-qPCR. Cell monolayers were harvested for **(C)** RT-qPCR analysis of viral RNA accumulation (n=3 statistical significance was determined by paired ratio t test; *, $p<0.05$; **, $p<0.01$; ns, non-significant).**(D)** 293T cells were infected as in (A) then treated with 5 or 10 µM 6-TG or DMSO. Lysates were harvested 24h after infection and were probed by western blotting as indicated. **(E)** 293T cells were grown on coverslips then infected with HCoV-OC43 and treated with 6-TG as in (A), then fixed and immunostained for N or **(F)** dsRNA. Nuclei are counterstained with Hoechst. Scale bar = 20 µm.

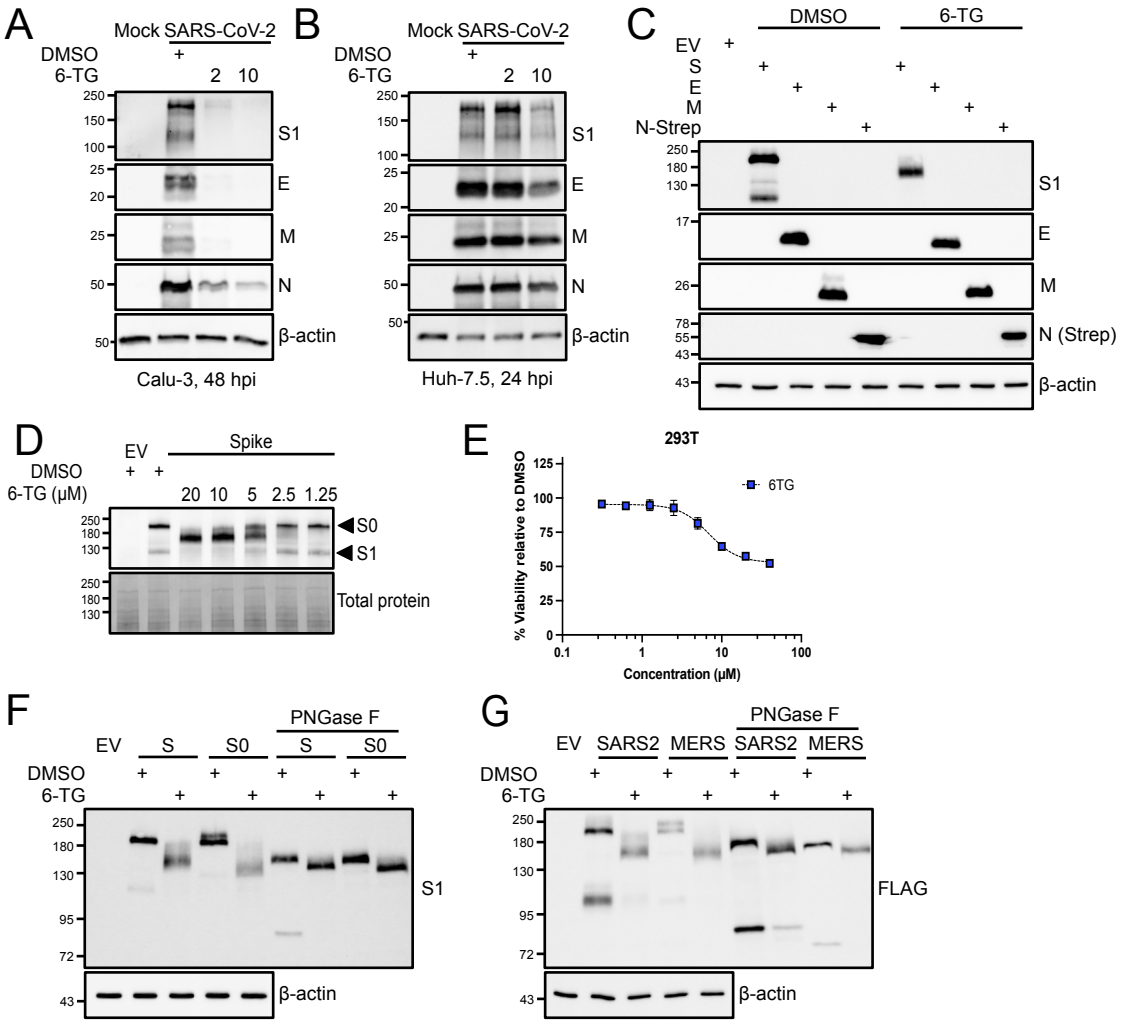

Figure 3. 6-TG inhibits Spike glycosylation and cleavage. **(A)** Calu-3 cells were infected with SARS-CoV-2 at an MOI of 7, then treated with 6-TG or DMSO. Lysates were harvested 48 h after infection and were probed by western blotting as indicated. Concentrations in legend are in μM. **(B)** Huh-7.5 cells were infected with SARS-CoV-2 at an MOI of 5, then treated with 6-TG or DMSO. Lysates were harvested 48 h after infection and were probed by western blotting as indicated. Concentrations in legend are in μM. **(C)** 293T cells were transfected with SARS-CoV-2 S, M, Envelope (E), Nucleoprotein (N) with a C-terminal 2xStrep tag, or EV then treated with 10 μM 6-TG or DMSO vehicle control. Lysates were harvested 24 h after transfection and probed by western blotting as indicated. **(D)** 293T cells were transfected with SARS-CoV-2 Spike or EV then treated with 6-TG or DMSO vehicle control. Lysates were harvested 24 h after transfection and were probed by western blotting as indicated. Concentrations in legend are in μM. **(E)** Alamar Blue cell viability assay of 6-TG treated 293T cells (n=3±SEM). **(F)** 293T cells were transfected with SARS-CoV-2 Spike (S), a Spike mutant lacking the Furin cleavage site between S1 and S2 (S0), or EV then treated with 10 μM 6-TG or DMSO vehicle control. Lysates were harvested 24 h after transfection, treated with PNGase F to remove N-linked glycans, and probed by western blotting as indicated. **(G)** as in (C) except 293T cells were transfected with C-terminal FLAG-tagged Spike (S-FL) or HCoV-MERS Spike (MERS).

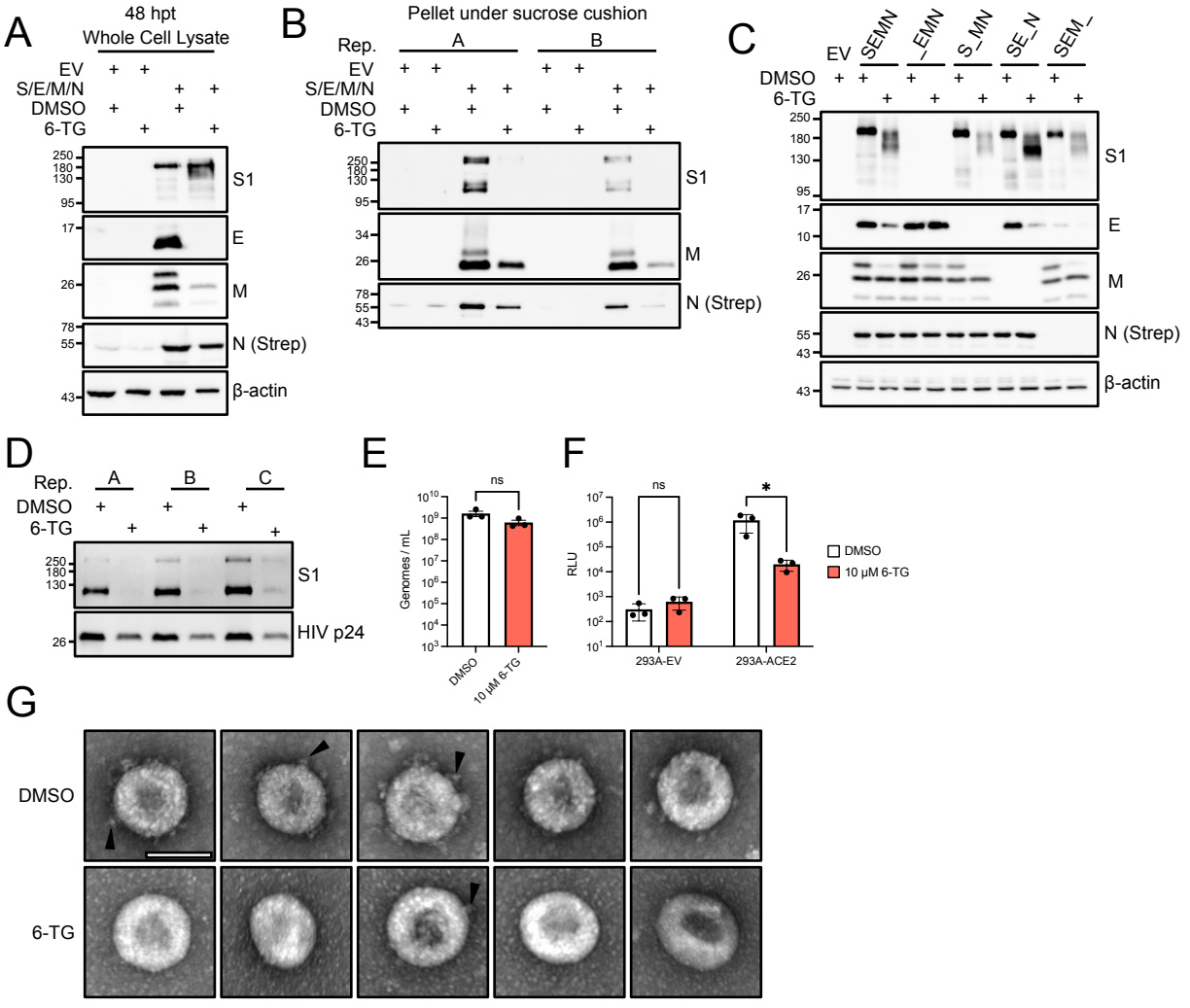

Figure 4. 6-TG stimulates an assembly defect and inhibits Spike virion incorporation. (A) 293T cells were transfected with equal quantities of SARS-CoV-2 S, M, E, and N plasmids or empty vector (EV) then treated with 10 µM 6-TG or DMSO vehicle control. Lysates were harvested 48 h after transfection and probed by western blotting as indicated. **(B)** Virus-like particles from supernatants of cells transfected in (B) were concentrated by ultracentrifugation through a 20% sucrose cushion, resuspended in PBS, then harvested with an equal volume of 2x Laemmli buffer. Samples from two independent lentivirus preparations were probed by western blotting as indicated. **(C)** 293T cells were transfected with S, E, M, and N in a 1:2:2:1 ratio, substituting one of the structural proteins for EV as indicated, treated with 6-TG or DMSO then processed as in (A). **(D)** SARS-CoV-2 Spike pseudotyped, luciferase-expressing lentivirus particles were concentrated by ultracentrifugation through a 20% sucrose cushion, resuspended in PBS, then harvested with an equal volume of 2x Laemmli buffer. Samples from three independent lentivirus preparations were probed by western blotting as indicated. **(E)** Genomes from three independent lentivirus preparations were quantified by RT-qPCR (n=3, statistical significance was determined by paired t-test; ns, non-significant). **(F)** 293A cells stably expressing ACE2 or empty vector control were transduced with lentivirus from three independent preparations. After 24 h, lysates were harvested and measured for luciferase activity (n=3, statistical significance was determined by two-way ANOVA; *, $p<0.05$; ns, non-significant). **(G)** 293A cells were infected HCoV-OC43 at an MOI of 0.1 =, then treated with 6-TG or DMSO. Supernatants were concentrated as in (C), before virions were fixed and imaged by TEM with negative staining. Five virions from both 6-TG- and DMSO-treated samples are shown at 150,000 X magnification. Scale bar = 100 nm. Arrowhead indicates examples of Spike protein extending from virion.

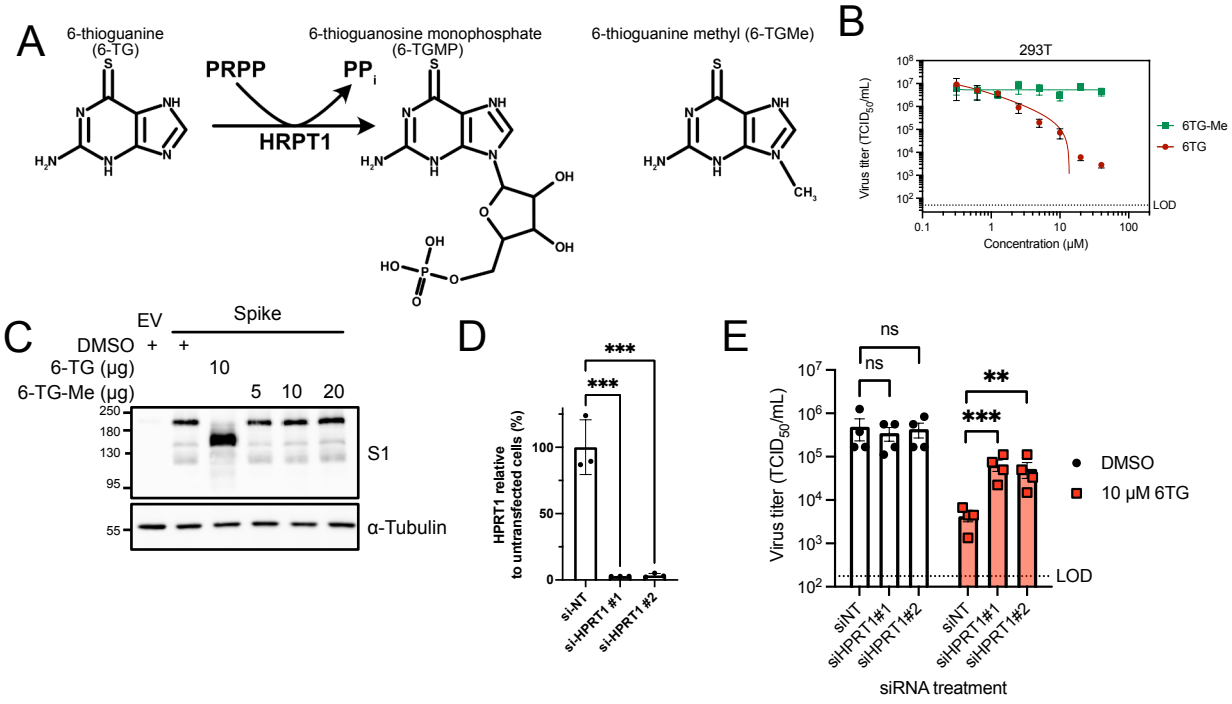

Figure 5. 6-TG inhibits Spike maturation through GTPase inhibition. (A) 6-TG is conjugated to phosphoribosyl diphosphate (PRPP) by HPRT1 to form 6-TG monophosphate. 6-TG methylated at the N9 nitrogen was designed to be resistant to processing by HPRT1. **(B)** 293T cells were infected with HCoV-OC43 at an MOI of 0.1 then treated with 6-TG or 6-TG-Me. Supernatant was harvested at 24 hpi and stored at -80°C until titering on BHK cells. (n=3 statistical significance was determined by paired ratio t test; *, $p<0.05$; **, $p<0.01$; ns, non-significant). **(C)** 293T cells were transfected with SARS-CoV-2 Spike or an empty vector control then treated with 6-TG, 6-TG-Me, or DMSO vehicle control. Lysates were harvested 24 h after transfection and probed by western blotting as indicated. **(D)** 293T cells were reversed transfected with siRNA and total RNA was harvested after 48 h. HPRT1mRNA abundance was measured by RT-qPCR (n=3, ±SEM statistical significance was determined by one way ANOVA; ***, $p<0.001$). **(E)** As in D but cells were infected with HCoV-OC43 at an MOI of 0.1 24 h after siRNA treatment and supernatant was harvested and titered as in **(B)** (n=4 ±SEM statistical significance was determined by paired ratio t test; **, $p<0.01$; ***, $p<0.001$; ns, non-significant).

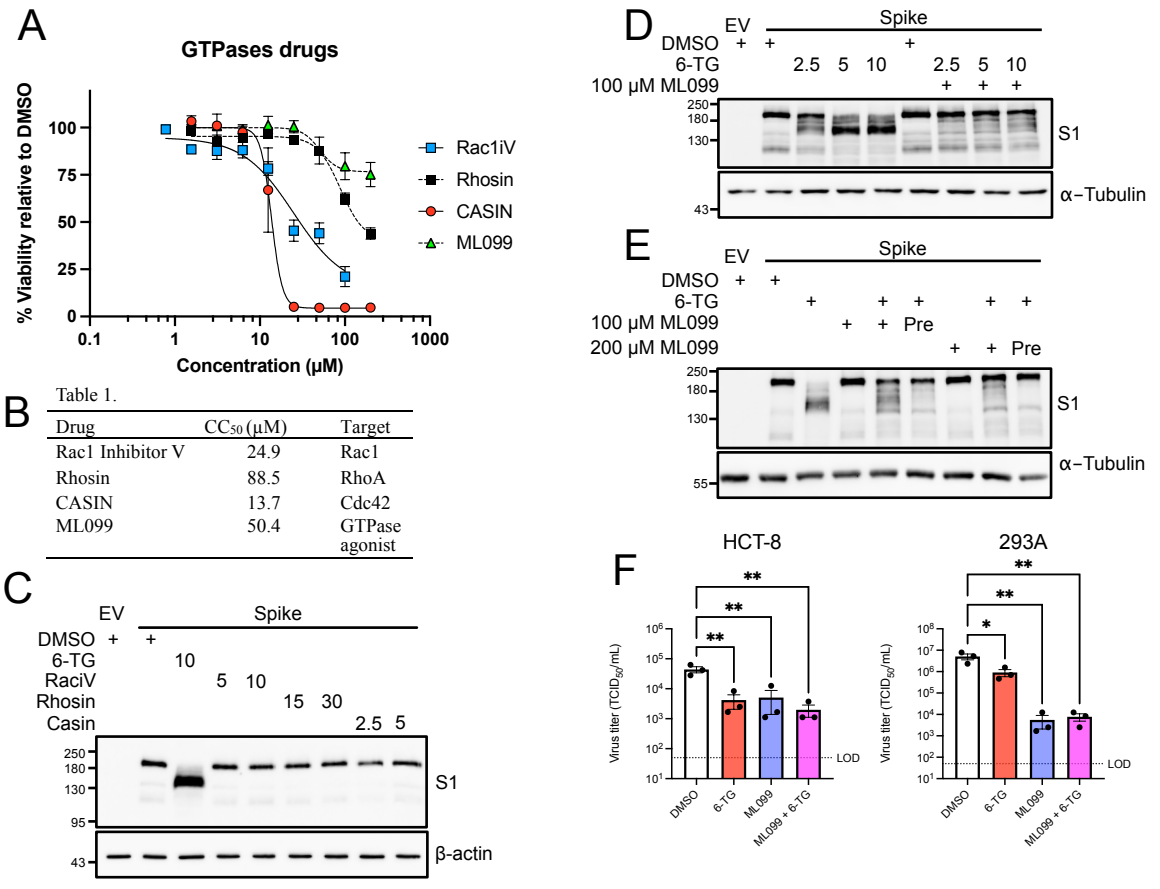

Figure 6. 6-TG inhibits Spike maturation through GTPase inhibition. (A) alamarBlue cell viability assay of 293T cells treated Rac1 Inhibitor V (Rac1iV), Rhosin, CASIN, or ML099 (n=3±SEM). **(B)** Summary table of 50% Cytotoxic concentration (CC_{50}) and inhibitor target of compounds tested in (A). **(C)** 293T cells were transfected with SARS-CoV-2 Spike or an empty vector control (EV) then treated with 6-TG, GTPase inhibitors, or DMSO vehicle control. Concentrations in legend are in µM. Lysates were harvested 24 h after transfection and were probed by western blotting as indicated. **(D)** 293T cells were transfected with plasmids encoding Spike or EV then co-treated with 6-TG, 100 µM ML099 GTPase agonist, or DMSO. Lysates were harvested 24 h after transfection and were probed by western blotting as indicated. Concentrations in legend are in µM. **(E)** as in (D) except some samples were pre-treated (Pre) for 4 h with ML099. **(F)** HCT-8 and 293A were infected with an MOI of ~0.1 then treated with 10 µM 6-TG or DMSO vehicle control. After 24 h, the supernatants was harvested and stored at -80°C until titering on BHK-21 (n=3 ± SEM, statistical significance was determined by one-way ANOVA; *, $p<0.05$; **, $p<0.01$; ns, non-significant). LoD = Limit of Detection for virus titer.

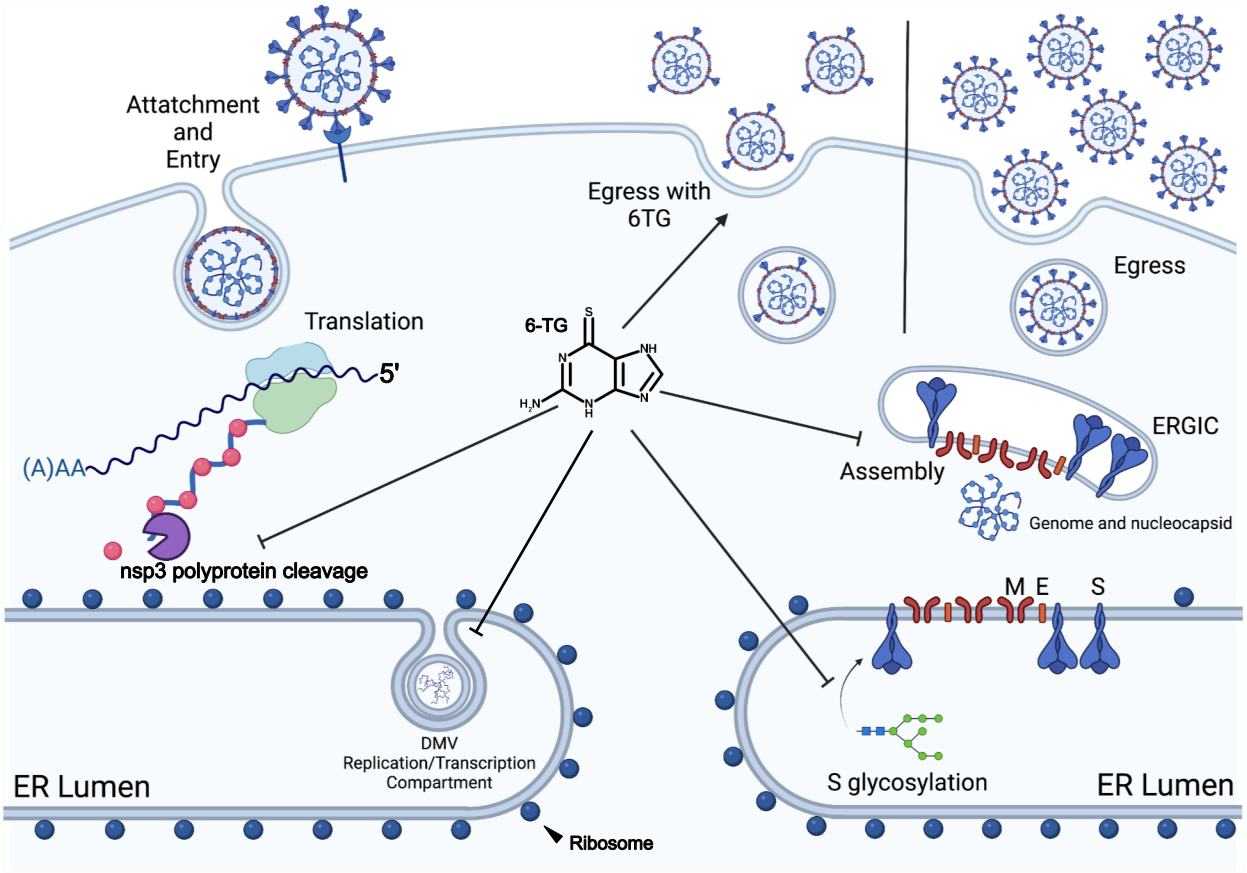

Figure 7. 6-TG inhibits multiple essential steps in virus replication and assembly. 6-TG inhibits nsp3, delaying formation of replication compartments and reducing accumulation of viral RNA. 6-TG also inhibits normal glycosylation of Spike, which fails to be properly packaged in egressing virions. As a result, the total number of virions released from infected cells is reduced and those that are released have fewer Spikes on their surface.

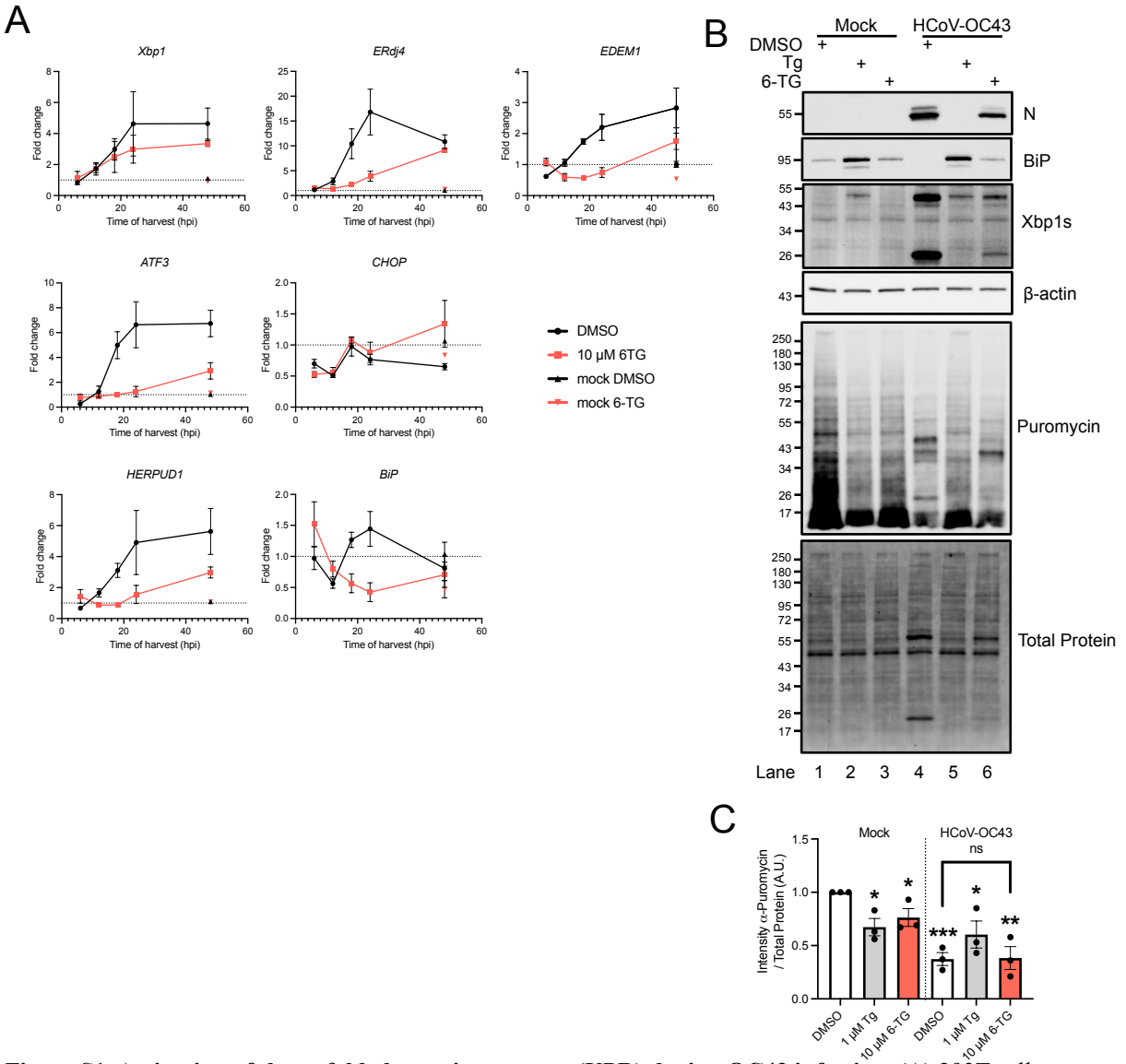

Figure S1. Activation of the unfolded protein response (UPR) during OC43 infection. (A) 293T cells were infected with HCoV-OC43 at an MOI of 0.1 then treated with 10 μM 6-TG or DMSO vehicle control. Total RNA from the cells were harvested at the times indicated and stored at -80°C until RT-qPCR analysis of UPR target genes. **(B)** 293A cells were infected as in (A), then treated with 10 μg 6-TG, 1μg thapsigargin (Tg), or DMSO. Cells were treated with 10 μg/mL of puromycin for 10 min prior to harvest 24 h after infection. Lysates were probed by western blot as indicated. **(C)** Total puromycin intensity from (E) was quantified relative to total protein load and are graphed normalized to the mock-infected, DMSO-treated cells (n=3 ± SEM, statistical significance was determined by paired t-test compared to mock-infected, DMSO-treated cells; *, $p<0.05$; **, $p<0.01$; ***, $p<0.001$; ns, non-significant).

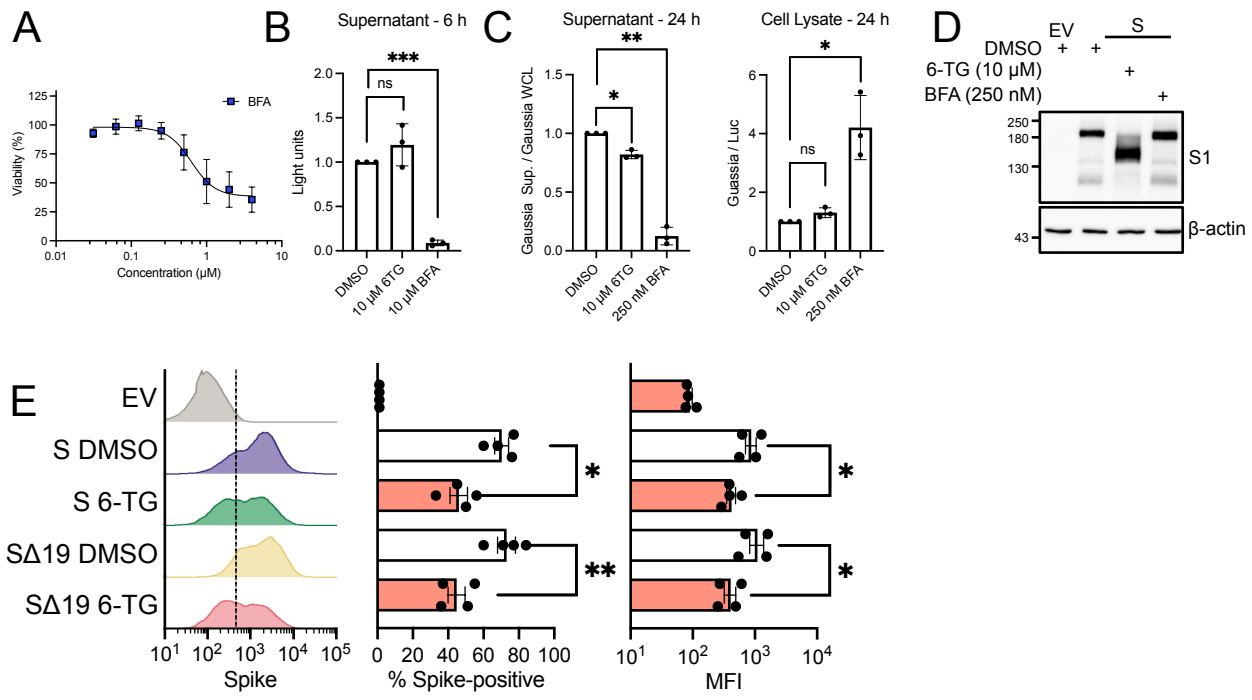

Figure S2. 6-TG reduces surface expression of Spike but does not globally limit secretion. (A) alamarBlue cell viability assay of 293T cells treated with brefeldin A (BFA) (n=4±SEM). **(B)** 293T cells were transfected with *Gaussia* luciferase for 18 h then treated with 6-TG, BFA or DMSO vehicle control for 6 h . Supernatants were recovered from the cells and measured for luciferase activity. **(C)** 293T cells were transfected with both luciferase and *Gaussia* luciferase then treated with 6-TG, BFA, or DMSO. After 24 h, supernatants were removed and analyzed as in (B). Cell lysate was harvested in Reporter Lysis Buffer and stored at -80°C until both luciferase and *Gaussia* luciferase activity was measured. (For B and C, n=3 ± SEM, statistical significance was determined by paired t-test compared to DMSO-treated cells; *, $p<0.05$; **, $p<0.01$; ***, $p<0.001$; ns, non-significant). **(D)** 293T cells were transfected with SARS-CoV-2 Spike or EV then treated with 6-TG, BFA, or DMSO. Lysates were harvested 24 h after transfection in 2x Laemmli buffer and were probed by western blotting as indicated. **(E)** 293T cells were co-transfected with EGFP and either Spike (S), Spike with 19 residue C-terminal truncation (SΔ19), or EV and then treated with 10 μM 6-TG or DMSO. After 24 h, cells were harvested, surface-stained for Spike then fixed prior to analysis by flow cytometry. EGFP+ cells were gated for analysis of number of Spike+ cells and Median Fluorescent Intensity (MFI) (n=4±SEM statistical significance was determined by paired t-test between 6-TG and DMSO treated cells; *, $p<0.05$).